Alma Mater Studiorum · Università di Bologna

Scuola di Scienze
Dipartimento di Fisica e Astronomia
Corso di Laurea in Fisica

First principles calculations of electronic properties of CsV_3Sb_5 kagome metal under doping

Relatore:
Prof. Domenico Di Sante

Correlatore:
Dr. Armando Consiglio

Presentata da:
Lorenzo Riguzzi

Anno Accademico 2023/2024

Abstract

I metalli kagome sono una famiglia di materiali quantistici il cui studio ha suscitato molto interesse negli ultimi anni a causa delle proprietà dovute al loro reticolo composto da esagoni e triangoli, detto, appunto, *reticolo kagome*. Questo reticolo induce la presenza di singolarità di Van Hove nelle strutture a bande di tali materiali, interessanti in quanto correlate a forti interazioni elettroniche, con conseguente possibilità di stato superconduttivo. Lo scopo di questa tesi è, tramite calcoli a principi primi, studiare le proprietà elettroniche del metallo kagome CsV_3Sb_5 sotto effetto di drogaggio con stagno (Sn) e tellurio (Te). Si partirà quindi con la spiegazione della *Density Functional Theory* (DFT), in particolare arrivando alla formulazione di Kohn e Sham e come questa consenta di ottenere la struttura a bande del materiale studiato. Successivamente verrà presentato il programma VASP (*Vienna Ab initio Simulation Package*), utilizzato per implementare il problema. Infine saranno riportati i risultati ottenuti nell'esperienza, mostrando sia che quelli ottenuti per CsV_3Sb_5 non drogato sono compatibili con quelli di precedenti studi, sia come l'effetto del drogaggio influenzi le singolarità di Van Hove di interesse, riuscendo, con entrambi i tipi di drogaggio, per livelli di drogaggio superiori al 5%, a portare allo spostamento di alcune di queste oltre il livello di Fermi, promuovendo effetti dovuti alla forte interazione fra gli elettroni associati a queste singolarità.

Abstract

Kagome metals are a family of quantum materials whose study has raised interest in recent years because of the properties related to their lattice made up of hexagons and triangles, called, in fact, *kagome lattice*. This lattice induces Van Hove singularities in the band structures of these materials, interesting since related to strong electronic interactions, with consequent possibility of superconducting state. The aim of this thesis is, through first principle calculations, to study the electronic properties of CsV_3Sb_5 kagome metal under doping with Tin (Sn) and Tellurium (Te). The starting point will be the explanation of *Density Functional Theory* (DFT), in particular obtaining Kohn and Sham formulation, and how this allows to derive the band structure of the material studied. Then VASP (*Vienna Ad initio Simulation Package*), which is the program used to implement the problem, will be introduced. Eventually the results of the experience will be reported, simultaneously showing that the results obtained for CsV_3Sb_5 without doping are compatible with those obtained by previous studies and that doping influences the Van Hove singularities of interest, succeeding, for both the types of doping, for doping levels greater that 5%, in shifting some of these singularities beyond the Fermi level, enhancing effects due to the strong interaction between the electrons related to these singularities.

Contents

Chapter 1

Introduction

In order to understand the methods and the results obtained from the study of the electronic properties of CsV_3Sb_5 kagome metal under doping, the following chapter includes some preliminary notions necessary for the comprehension of the work. These notions include what band structures and Van Hove singularities are and what properties characterizes superconductors, since many studies carried out on CsV_3Sb_5 had the aim of studying properties such as its critical temperature and field and the interplay between the superconducting state and the charge density wave state. Eventually a brief account of these previous studies and their results is reported, in order to show what has been studied so far and what are the properties that have been observed.

1.1 Band structures

An isolated atom shows a discrete set of energy levels, which tend to become continuous by increasing the distance of the electrons from the nucleus. Bringing two atoms close to each other will make the orbitals of the single atoms merge to create molecular orbitals. Keeping on adding atoms more and more molecular orbitals will be created, with energies close to each other (Fig. 1.1).

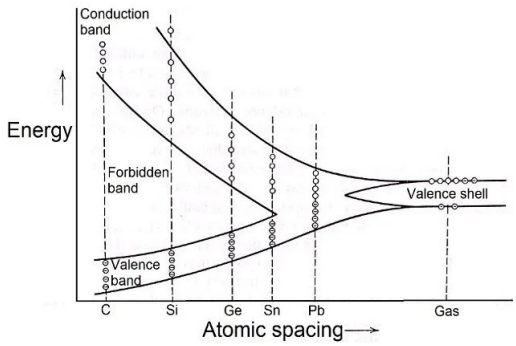

Figure 1.1: *Energy levels as a function of the distance between atoms. For high distances the system behaves as a gas and the levels are discrete, while when decreasing the distance the energy levels change into energy bands with continuous levels. Keeping on lowering the distance the energy levels split into two bands, the conduction band and the valence band, separated by a gap of forbidden energy levels. The amplitude of this gap allows to divide materials into insulators (as Carbon in Figure), semiconductors (as Silicon and Germanium in Figure) and conductors (as Lead in Figure).*

For a periodic system the number of atoms becomes infinite and one can define a unit cell with a known number of atoms which is repeated in space. These kinds of systems will thus have translational symmetries and the Hamiltonian will include a periodic potential $V(\vec{r}) = V(\vec{r} + \vec{a})$, where $\vec{a}$ is the lattice step. Because of this potential also the Hamiltonian will be periodical with the same periodicity and from *Bloch theorem* wavefunctions will be of the form:

$$\Psi(\vec{r}) = e^{i\vec{k}\cdot\vec{r}}u(\vec{r}) \tag{1.1}$$

where $\vec{k}$ is the wavevector of a single electron in the first Brillouin Zone and $u(\vec{r})$ is a function with the same periodicity of the lattice and depends on the orbitals considered. It is easy to prove that for this *Bloch wavefunction* a translation of a lattice vector $\vec{a}$ implies a modulation of the wavefunction only by a phase factor:

$$\Psi(\vec{r} + \vec{a}) = e^{i\vec{k}\cdot\vec{a}}\Psi(\vec{r}) \tag{1.2}$$

Energy bands graphs plot the energy levels of the electrons as functions of the wavevector $\vec{k}$, in the reciprocal space[1]. Considering, for example, s orbitals for a one-dimensional Hydrogen chain of step a, the point $k = 0$, called Γ, corresponds, from eq. 1.2, to a configuration where $\Psi(r + a) = \Psi(r)$ and all the orbitals have the same phase. This corresponds to a configuration of minimal energy, because of the absence of nodes. Moving in the reciprocal space at $ka = \pi$ the wavefunction becomes $\Psi(r + a) = -\Psi(r)$, which means that, in this configuration, atoms close to each other have opposite phases leading to an increase in the energy eigenvalues. The graph $E(k)$, named band structure, for this example is shown in Fig. 1.2.

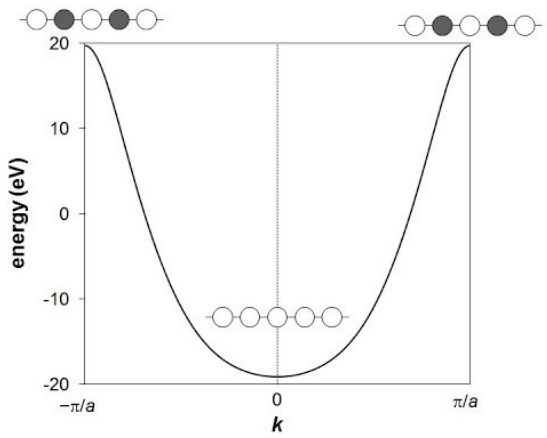

Figure 1.2: *Band structure of a chain of Hydrogen atoms with step a.*

Similar considerations can be done for other kinds of orbitals.
The energy eigenstates at a certain value of $\vec{k}$ with a certain energy have contributions that come from different orbitals. This means that different orbitals of each atom will contribute differently to these eigenstates. Considering CsV_3Sb_5 as an example, the Cs atom will have s orbitals, which are located close to the nucleus and will contribute only to high energy eigenvalues[2], while V will contribute with d orbitals and Sb with p

[1]For the uncertainty principle, assigning an exact wavevector to an electron means that the electron is considered delocalized in the whole real space.

[2]Cs has a mainly structural contribution and is needed in order to have null valence.

orbitals. Since there are 5 different types of $3d$ orbitals ($d_{xy}, d_{xz}, d_{yz}, d_{x^2-y^2}, d_{z^2}$) and 3 of $5p$ orbitals (p_x, p_y, p_z) and the unit cell includes 3 V atoms and 5 Sb atoms, the low energy physics will have contributions from 15 orbitals for each element.

In a crystal electrons are located in different energy bands separated by energy regions where there are no orbitals allowed (energy gaps). These structures make it possible to divide materials into 3 different categories, based on the occupation of these bands ([1], pg. 163):

- Insulators and semiconductors: all energy bands are either full or empty;
- Conductors: one or more bands are partially full or empty;

1.2 Van Hove singularities

Van Hove singularities (VHs) are singularities in the density of states of crystals, where the density of states diverges logarithmically.
The density of states $g(E) = dN/dE$ represents the number of energy states allowed in the range $[E, E + dE]$.

The density of states for a crystal lattice can be expressed as (see [2]):

$$g(E) = \int_{BZ} \frac{d^3k}{(2\pi)^3} \delta[E(\vec{k}) - E] \tag{1.3}$$

where the integral is extended to the first Brillouin Zone.
It is known that for Dirac delta function holds:

$$\int_a^b g(x)\delta[f(x)]dx = \sum_{x_0} g(x_0) \left| \frac{df}{dx} \right|^{-1}_{x=x_0}$$

where x_0 is a zero of $f(x)$ in the interval $]a, b[$.
This allows to rewrite eq. 1.3 as:

$$g(E) = \frac{1}{(2\pi)^3} \int_{E(\vec{k})=E} \frac{dS}{|\nabla_{\vec{k}} E(\vec{k})|}$$

where dS is an element of the surface in the $k - space$ where $E(\vec{k}) = E$.
This result shows that the singularities in $g(E)$ originate from the critical points of $E(\vec{k})$. Its behaviour is different depending on the kind of critical point that is being considered and can be found expanding $E(\vec{k})$ in Taylor series near the critical point E_0. Kagome materials have 2D structures and the behaviour of the density of states of these lattices in proximity of a saddle point of an energy band was described by *Van Hove L.* [3]:

$$g(E) \propto ln \left| 1 - \frac{E}{E_0} \right|$$

and shows a logarithmic divergence.
It can be proved that the effective masses of the electrons for a given *k-point* of the

energy bands are proportional to the inverse of the second derivative of the band at that point (see [4]). Since VHs correspond to the saddle points of the energy bands, where the second derivative of the band is 0, electrons in such points will behave as if they have an infinite effective mass, which results in very slow electrons, enhancing their possibility of interacting with each other.

1.3 Superconductivity

1.3.1 Phenomenological observations

The superconducting state is a state of matter observed at very low temperatures where the electrical resistivity is zero, which means that the flow of electrical current in such materials is allowed without attenuation. Indeed persistent electrical currents have been observed to flow without attenuation in superconducting rings for more than a year [1]. This particular property is shown under a critical temperature T_C together with other phenomenological observations, such as the *Meissner effect*, which is the expulsion of $\vec{B}$ lines in a superconductor cooled below T_C in a magnetic field, so that the superconductor behaves as if $\vec{B} = \vec{0}$ inside it. In order to screen an external magnetic field $\vec{B_a}$ the magnetization $\vec{M}$ inside the superconductor must satisfy: $\vec{B} = \vec{B_a} + 4\pi\vec{M} = \vec{0}$.
From *Ohm's law*: $\vec{E} = \rho\vec{j}$, which leads to $\vec{E} = \vec{0}$ for $\rho = 0$, and, from *Faraday-Neummann-Lenz's law*: $\nabla \wedge \vec{E} = -\partial\vec{B}/\partial t$, which implies $\partial\vec{B}/\partial t = \vec{0}$, but not $\vec{B} = \vec{0}$. This means that perfect diamagnetism is an essential property of the superconducting state.
In addition to this, a sufficiently strong magnetic field $H_C(T)$ (which depends on the temperature), will destroy the superconducting state. For this magnetic field holds: $H_C(T_C) = 0$.
These properties divide superconductors in two categories:

- Type I superconductors: pure specimens of materials, with low values of T_C and H_C;
- Type II superconductors: alloys or transition metals, for which T_C is generally higher and the *Meissner effect* holds till a critical field H_{C1}. This type of superconductors still show superconducting properties until a second magnetic field H_{C2} is reached, but with a magnetic field flux different from 0 inside the material (this region is called *vortex state*).

The differences between the two types of superconductors are shown in Fig. 1.3.

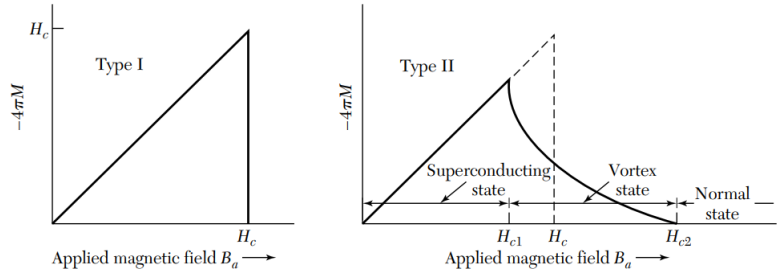

Figure 1.3: *Behaviour of the two different types of superconductors under an external magnetic field B_a. Image taken from* [1].

In all superconductors entropy decreases markedly on cooling down below T_C, which means that the superconducting state is more ordered than the normal state, so the electrons thermally exited in the normal state are more ordered in the superconducting state. This means that only a small fraction of the conduction electrons participates in the transition to the ordered superconducting state.

1.3.2 BCS theory of superconductivity

The quantum theory of superconductivity was developed by Bardeen, Cooper and Schriefler. This theory is based on the electron-lattice-electron interaction, which leads to an indirect interaction between two electrons. The crystal lattice can be described as positive ions in well-defined positions, whose behaviour can be described by quantum harmonic oscillators. During its motion in the lattice the first electron will provoke a displacement of some of the ions in the lattice due to its negative charge. This displacement will cause a local positive charge density accumulation in the nearby of these ions, which will last for a certain time since the positive ions will take some time in order to return to their original positions. This positive charge density may attract the second electron, which will thus follow the first one, forming the so called *Cooper pair*.

The ground state of a gas of free electrons is given by the Fermi-Dirac distribution, which for $T = 0$ leads to a state where only the states under the Fermi level E_F are occupied by electrons. One can imagine to raise one electron above E_F and, for an appropriate attractive interaction between electrons, the new ground state will be superconducting and separated by a finite energy E_g from the previous one (Fig. 1.4).

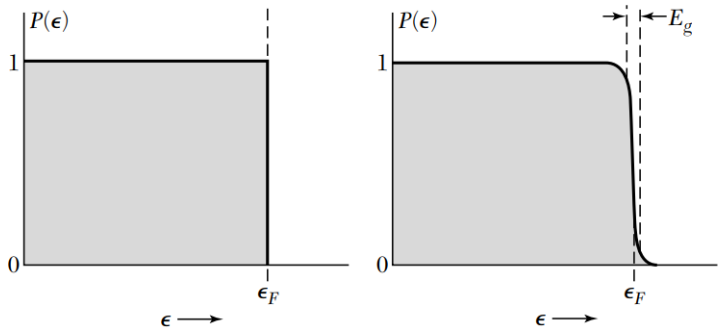

Figure 1.4: *Comparison between the ground state of the non-interacting electron gas (left) and the BCS ground state (right), which differs from the Fermi state in a region of width of the order of the energy gap E_g. Both curves are for absolute zero. Image taken from* [1].

The main feature of the BCS theory is the *Cooper pair*, described by a singlet two-particle wavefunction formed by a spin up electron with wavevector $\vec{k}$ and a spin down electron with wavevector $-\vec{k}$. *Cooper pairs* have total spin 0 and as such behave as bosons.

The attractive interaction between the electrons in the cooper pair is mediated by a particle named phonon, which allows the two electrons to exchange energy and momentum. In order to obtain this, one can consider the Hamiltonian of a 1 dimensional crystal lattice of step a as the Hamiltonian of a system of harmonic oscillators with periodic boundary conditions:

$$\hat{H} = \sum_i \frac{p_i^2}{2m} + \frac{1}{2} m\omega^2 \sum_i (x_i - x_{i+1})^2$$

The periodic boundary conditions allow to express the position and momentum operators as Fourier series (see [5]). Working now in the $k-space$ the creation and destruction operators can be defined as:

$$a_k = \left(\frac{m\omega_k}{2\hbar}\right)^{1/2} \left(x_k + \frac{i}{m\omega_k} p_{-k}\right)$$

$$a_k^\dagger = \left(\frac{m\omega_k}{2\hbar}\right)^{1/2} \left(x_k - \frac{i}{m\omega_k} p_{-k}\right)$$

where $\omega_k = 2\omega|\sin(ka/2)|$ and x_k and p_k are the Fourier transforms of x_i and p_i. Substituting these in the Hamiltonian of the system gives:

$$\hat{H} = \sum_k \hbar\omega_k \left(a_k^\dagger a_k + \frac{1}{2}\right) \tag{1.4}$$

This shows that the system is described by an independent harmonic quantum oscillator for each value of k so that the interaction is mediated by particles called phonons which allow the exchange of momentum and are described by creation and destruction operators which act on states with different values of k.
Considering now a system of both electrons with wavevectors labelled by $\vec{k}$ and phonons with wavevectors labelled by $\vec{q}$, the Hamiltonian of the system will include both the Hamiltonians of the free electrons and of the free phonons (eq. 1.4) and an interaction term:

$$\hat{H} = \sum_{k,\sigma} \frac{\hbar^2 k^2}{2m} c_{k,\sigma}^\dagger c_{k,\sigma} + \sum_{q,\lambda} \hbar\omega_{q,\lambda} \left(a_{q,\lambda}^\dagger a_{q,\lambda} + \frac{1}{2}\right) + \frac{1}{V} \sum_{k,\sigma} \sum_{q,\lambda} g_{q,\lambda} c_{k+q,\sigma}^\dagger c_{k,\sigma} (a_{q,\lambda} + a_{-q,\lambda}^\dagger)$$

where the first term is the free electron Hamiltonian, the second one is the free phonon Hamiltonian given by eq. 1.4 and the last one is the interaction term, where $g_{q,\lambda}$ is the coupling strength of the electron-phonon interaction. The index λ represents the phonon possible polarizations and allows to pass from the 1-dimensional system considered in order to obtain Hamiltonian 1.4 to a three dimensional system, while σ represents the spin dependence.

The BCS ground state will thus be a phase coherent superposition of *Cooper pairs* of electrons with momenta $(k, -k)$ [6]:

$$|\Psi_{BCS}\rangle = \prod_k (u_k + v_k c_k^\dagger c_{-k}^\dagger)\,|0\rangle$$

where $|0\rangle$ is the empty state and v_k and u_k are coefficients whose square moduli represent the probability that a pair with one electron with momentum $\vec{k}$ and the other one with momentum $-\vec{k}$ exists or not and are such that $|u_k|^2 + |v_k|^2 = 1$. These coefficients must minimize the expectation value of $\langle\Psi_{BCS}|\,\hat{H}\,|\Psi_{BCS}\rangle$, where the Hamiltonian is given by [6]:

$$\hat{H} = \sum_{k\sigma} \epsilon_k c_{k\sigma}^\dagger c_{k\sigma} + \frac{1}{N} \sum_{kk'} U_{kk'} c_k^\dagger c_{-k}^\dagger c_{-k'} c_{k'}$$

where $\epsilon_k = E_k - E_F$ is the energy with respect to the Fermi level and $U_{kk'}$ is the potential responsible for a transition from an initial state $(k, -k)$ to a final state $(k', -k')$ and depends on the attractive potential that allows the formation of the *Cooper pairs*. This potential will be active only for electrons with energies in the range $[E_F, E_F + \hbar\omega_D]$, where ω_D is the Debye frequency of the material. Usually, $E_F \sim 1eV$ and $\hbar\omega_D \sim 1meV$. The binding energy of the *Cooper pair* is proportional to ω_D and strongly suppressed by an exponential factor which depends on the inverse of the product of the electron-phonon coupling energy and the density of states at the Fermi level of the metal. This means that, as long as the density of states is finite, the configuration of the Cooper pair is more convenient, even for low values of the coupling energy. The form of $U_{kk'}$ depends on the type of superconductor considered.
The wavefunction obtained by solving this variational principle and this Hamiltonian can be used to describe many of the properties observed for superconductors.

1.4 Kagome materials

Kagome materials are quantum materials characterized by a 2D atomic lattice constructed by regular hexagons surrounded by corner-sharing triangles, which resembles the kagome pattern in Japanese basket-weaving, from which they take their name (Fig. 1.5b). Because of this triangular arrangement, kagome lattices, combined with a spin degree-of-freedom, exhibit a frustrated behaviour. Indeed, since spin has 2 degrees of freedom (↑ and ↓), given the spin configuration for two of the three vertices, the third one is undefined and the ground state of the system is a linear combination of two different states (Fig. 1.5a).

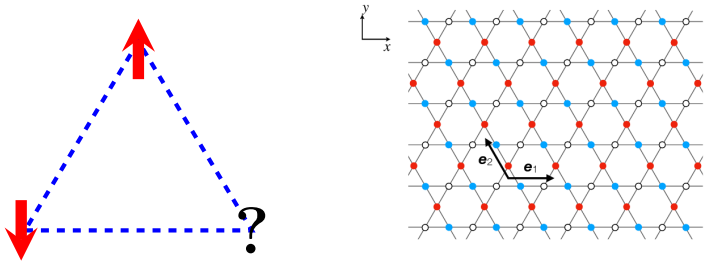

(a) (b)

Figure 1.5: ***a)*** *Visual representation of a frustrated triangular system. Chosen the direction of two spins, constrained to be collinear, the third one is undefined, since it would either be aligned with one of the others, which are at the same distance from it.* ***b)*** *Example of an ideal kagome lattice. Image taken from* [7].

The first kagome studied were actually insulators. Examples of such materials are herberthsmithite and kapellasite [8]. These materials are characterized by the presence of copper, whose $3d$ orbitals are close to the nucleus, with consequent presence of strong Coulomb interactions between electrons in this orbital and the nucleus. In these kind of systems non-collinear magnetism can be observed [8].
In 2018, with FeSn and Fe_3Sn_2, the first cases of kagome with metallic features were observed.
AV_3Sb_5 kagomes, where A is an alkaline metal, has been studied since 2020. In the case studied in this thesis the alkaline metal will be Cs. In this kind of kagomes the kagome

lattice is made by the vanadium atoms, which still has $3d$ orbitals. The V-Sb covalent network is intercalated by a triangular network of alkali metal ions (Fig. 1.6b) and there are two distinct sublattices of Antimony, where the Sb atom sitting within the kagome network occupies a different *Wyckoff position* compared to the Sb atoms above/below the kagome plane [9] (Fig. 1.6a). These kagomes have a quasi-two dimensional structure both chemically and electronically, as it will be shown and discussed in the next sections.

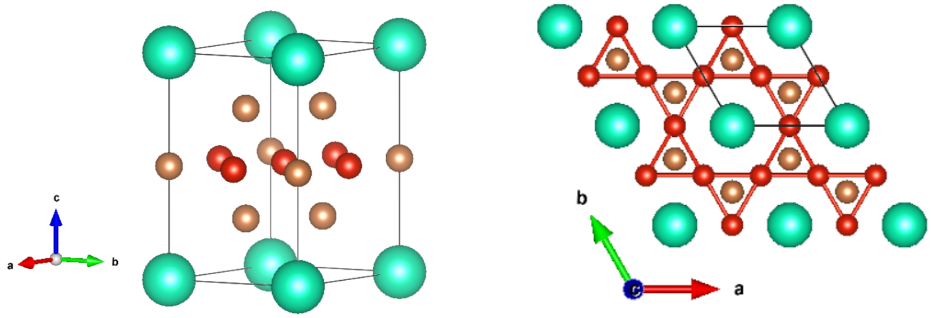

(a) *Unit cell of CsV_3Sb_5* (b) *Kagome network in CsV_3Sb_5*

Figure 1.6: *Lattice structure of CsV_3Sb_5: cyan spheres represent the Cs atoms, red spheres shows the kagome network made by V atoms each coordinated by an octahedra of Sb atoms depicted as bronze spheres.*

The kagome sheets are well isolated, resulting in a quasi-two dimensional structure, which allows single crystals to be highly exfoliable [9]. In addition to this, AV_3Sb_5 family is highly tolerant of air, water, and common solvents [9], increasing the overall accessibility of experiments using single crystals.

The kagome network in the AsV_3Sb_5 family can lead to interference effects whose details depend on the position of the Fermi level relative to singularities in the electronic band structure. Specifically the kagome network generates bands with saddle points at electron fillings $f = 5/12$ and $f = 3/12$ (Fig. 1.7) where long-range Coulomb interactions can be promoted due to sublattice interference effects, due to the fact that not only the eigenvalues that generate the band at that point are important, but also the eigenvectors associated to them.

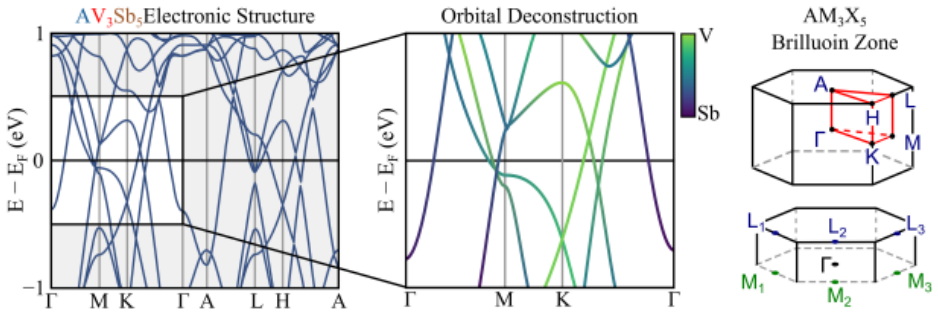

Figure 1.7: *Band structure of kagome metals of the family AV_3Sb_5 determined with density functional theory calculations, with highlight on the two saddle points with V orbital character just below E_F at the M-point and the mixed (V,Sb) character saddle point above E_F at the M-point. On the right the BZ is illustrated, with the location of high-symmetry points labelled. Image taken from* [9].

These VHs generate a logarithmic divergence in the density of states at the M-points of the BZ, which occur in different flavours. The VHs at $f = 5/12$ is called pure type or *p-type* VHs and its wavefunctions derives from a single V atom. The one at $f = 3/12$, instead, is called mixed type or *m-type* VHs and its wavefunction derive from both the other two V atoms (Fig. 1.8).

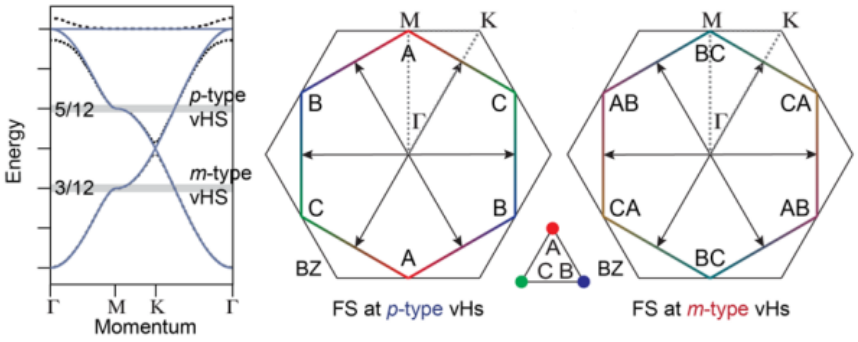

Figure 1.8: *Two different types of VHs in the band structure of a prototypical kagome lattice and Fermi surface of the kagome lattice at the two considered VHs. The three different colors represent the different contributions of the 3 atoms. Image taken from* [10].

Fig. 1.8 also shows that the three M points of the BZ are inequivalent, from the point of view of the eigenstates, since the contribution to the VHs for each of them comes from different V atoms (labelled in Fig. 1.8 with A, B and C), so that the eigenstate of each of them will be different.

Due to structural instabilities the previously shown configuration of the AV_3Sb_5 compounds (also named *"Pristine"*) can exhibit two structural distortions of the V sublattice, which maps them into energetically favored modes of the kagome plane. This distortions are accompanied by modulations in the local density of states. These configurations are known as: *"Star of David"*, where the 3 V atoms move away from each other, and *"Inverse star of David"* (Fig. 1.9). Both of them are energetically more convenient and can be reached lowering the temperature, but the *"Inverse Star of David"* is energetically more convenient than the *"Star of David"*. This modulation of the plane leads to the breaking of rotational symmetry.

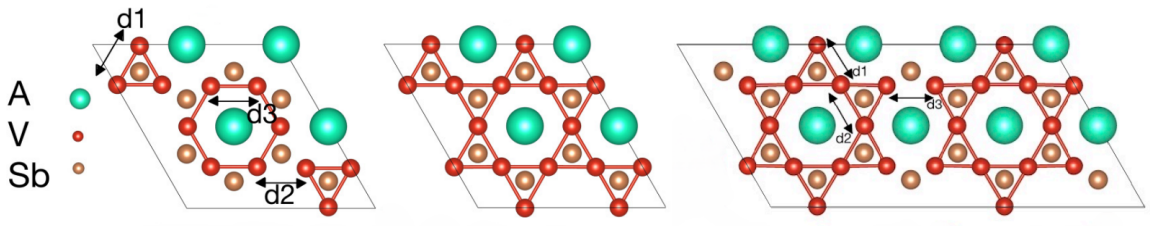

Figure 1.9: *Comparison of the two configurations of the kagome network in AV_3Sb_5 compounds. The "Pristine" configuration is shown in the middle, while the "Inverse Star of David" is shown on the left and the "Star of David" on the right. Image taken from* [11].

The change in the configuration from *"Pristine"* to *"Inverse Star of David"* (or *"Star*

of David") can be described by *Landau theory of phase transitions*. In this theory the free energy of the system is a function of temperature and an *order parameter* Δ, which is a thermodynamic variable that is zero on one side of the transition and non-zero on the other one: $F = F(\Delta, T)$. For superconductors or superfluids the order parameter is the amplitude of the superconducting wavefunction $|\Psi|^2$ and F can be expanded in Taylor series of this *order parameter*, including only terms allowed by symmetry:

$$F = \alpha|\Psi|^2 + \frac{\beta}{2}|\Psi|^4$$

where α and β are T-dependent coefficients. Assuming $\beta = const > 0$, for $\alpha > 0$ F has a single minimum at $|\Psi| = 0$, while for $\alpha < 0$ it has a local maximum for $|\Psi| = 0$ and two minima symmetric with respect to the vertical axis and of the same amplitude. Expanding α at leading order in T: $\alpha = a(T - T_C)$, where $a > 0$. This means that the phase transition from the configuration with one minimum, to the one with two minima occurs when passing from $T > T_C$ to $T < T_C$ (Fig. 1.10a). The description of this phase transition for kagome materials includes some complications and, for symmetry considerations due to their crystal lattice, the free energy, for $T < T_C$, shows two minima with different amplitudes. The minimum with the lower energy will correspond to the *"Inverse star of David"* and the other one to the *"Star of David"*, while the point corresponding to $|\Psi| = 0$ will correspond to the *"Pristine"* configuration (Fig. 1.10b).

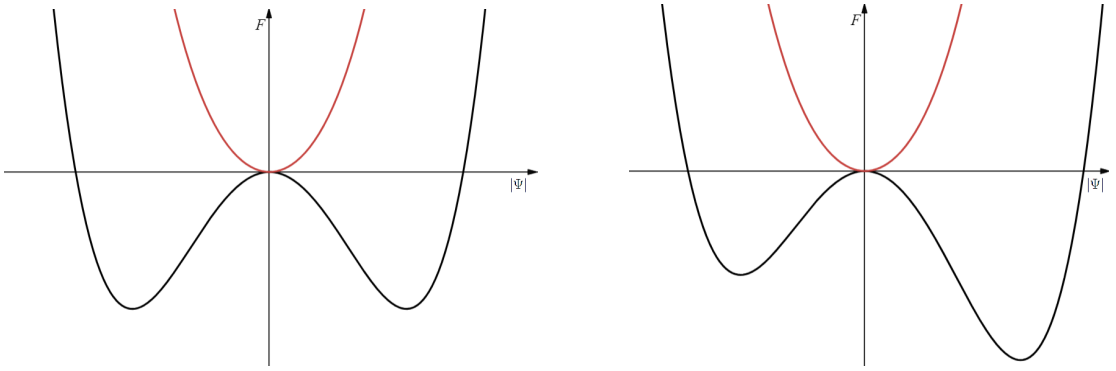

(a) *Behaviour of the free energy during the phase transition in Landau Theory*

(b) *Free energy during the phase transition for kagome materials.*

Figure 1.10: *Behaviour of the free energy as a function of the order parameter. The red graph corresponds to the configuration for $T > T_C$, while the black graph for $T > T_C$. In the graph on the right, for kagome materials, the origin of the axis corresponds to the "Pristine" configuration, the lower minimum to the "Inverse Star of David" and the other one to the "Star of David".*

1.5 Electronic properties of CsV_3Sb_5

1.5.1 Band structure and Van Hove singularities

The diverging density of states of the VHs at the M-point near the Fermi level might be the driving force of charge order and superconductivity in CsV_3Sb_5.

Once the filling corresponding to a VHs is reached, nesting between the three inequivalent M-points across the Fermi surface is predicted to promote a number of charge/spin

density wave and superconducting instabilities. The band structure of CsV_3Sb_5 is shown in Fig. 1.11.

Bands at the Fermi level are dominated by states arising from the kagome nets of Vanadium *d*-states. These are multi-orbital materials with d_{xy}, d_{yz} and d_{xz} derived bands forming a series of *m-type* and *p-type* VHs at the M-points of the BZ at energies reasonably close to E_F. In CsV_3Sb_5, states that are identified with the *m-type* d_{xz}, d_{yz} VHs are nearly perfectly nested. Optical conductivity data resolve the partial gap that opens below the CDW transition to be $\Delta_{CDW} \approx 78meV$, with $T_{CDW} = 94K$ [9]. Additional states at E_F originating from Sb *p*-orbitals likely also play a role. The large electron pocket at the Γ-point is generated by *p*-orbitals from the Sb sites in the kagome plane (in the centers of the hexagons of the kagome nets), and an M-point VHs of mixed Sb/V character that appears slightly above E_F derives from a mixture of V-states with out-of-plane Sb *p*-state.

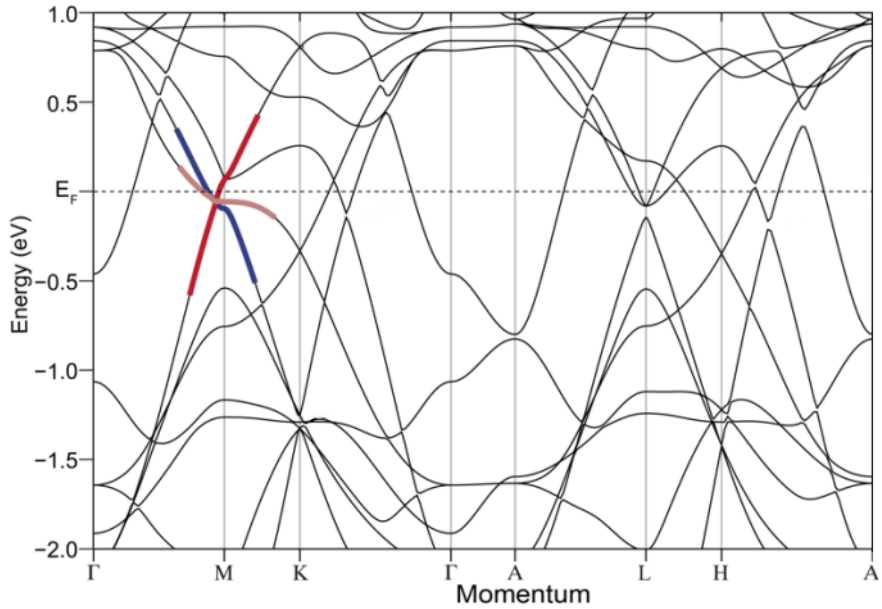

Figure 1.11: *Theoretical electronic structure of CsV_3Sb_5 from Density Functional Theory. The Fermi level was set to 0.0eV. Some of the VHs near the Fermi level are highlighted. The VHs highlighted in pink is of p-type, while the one at point M slightly above the Fermi level highlighted in red is of m-type. Image taken from* [10].

The type of the VHs is critical to understand the unconventional many-body phases emerging from the kagome lattice as it determines the momentum dependence of the bare susceptibility (a detailed expression for this dependence and its explanation can be found in the supplementary materials of [12]) and the electron-electron (electron-hole) pairing symmetries, which is the symmetry of the wavefunction of the *Cooper pairs* in the *k-space*, of the superconducting (charge ordered) state (for detailed info see [12]). The *m-type* VHs from the odd parity d_{xz}/d_{yz} kagome band contributes to the formation of charge order by promoting Fermi surface nesting, while the *p-type* VHs from the $d_{xy}/d_{x^2-y^2}$ kagome band contributes via higher-order VHs (with power-law diverging density of states) and enhanced density of states.
For the Inverse star of David configuration charge order is shown below $T_{CO} = 78 \sim 102K$ and superconductivity below $T_C = 0.92 \sim 2.5K$. CsV_3Sb_5 seemingly possesses mixture of the two configurations layered relative to one another.

CsV_3Sb_5 hosts superconducting transition within the Charge Density Wave state, with $T_C = 2.5K$. Different types of superconductivity are predicted to emerge due to nested VHs in the kagome band structure.

1.5.2 Phase diagram

High pressure is a clean method to tune the electronic properties without introducing any impurities, and pressure is often used as a control parameter to tune superconductivity and charge density wave state. Maximum T_c of $8K$ is observed at $P_2 \approx 2GPa$ when charge density wave is completely suppressed. Strikingly, an unusual suppression of superconductivity is observed between $P_1 \approx 0.7GPa$ and $P_2 \approx 2GPa$. These results indicate an unexpected competition between charge density wave and superconductivity in this region. The behaviour of this competition is shown in Fig. 1.12.

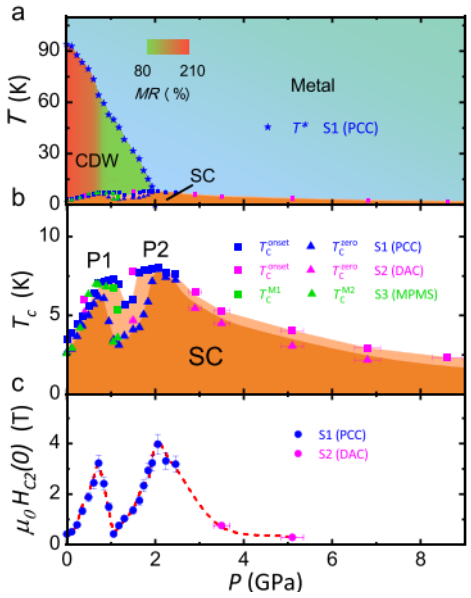

Figure 1.12: ***a)*** *Phase Diagram of CsV_3Sb_5 with temperature against pressure;* ***b)*** *Pressure dependence of superconducting transition temperature;* ***c)*** *Pressure dependence of upper critical field at zero temperature. Image taken from* [13].

The charge density wave transition temperature gradually decreases while increasing the pressure, while the superconducting transition temperature increases with increasing the pressure below P_1, then decreases suddenly and becomes sharp again at P_2, showing the highest $T_C \approx 8K$. After this it is again suppressed for increasing pressure.
The upper critical field H_{C2} shows a similar behaviour (Fig 1.12c).

Perturbing the charge density wave state via external pressure or chemical doping can have a dramatic effect on the superconducting phase, indeed the competition between charge density wave state and superconductivity is usual since the gap opening at charge density wave state reduces the density of states at Fermi surfaces, leading to the suppression of superconductivity [13]. T_C is enhanced as the charge density wave state is suppressed and frees up a greater density of states for the superconducting condensate. This suppression of charge density wave state terminates with the maximization of T_C. Pressure acts like a perturbation that leads to the suppression of charge density wave

state, affecting the VHs near the Fermi level and thus enhancing the superconducting state.

Doping CsV_3Sb_5 is another kind of perturbation which may have effects on the position of the VHs with respect to E_F. This is the case studied in this thesis, where, in particular, Sb atoms have been replaced with Te and Sn atoms at different levels of doping.

Chapter 2

The many-electron problem

Studying the quantum properties of a material means studying its Schrödinger equation, which means that the starting point of the study developed in this thesis will be a many-body Schrödinger equation. However the solution of this problem will be too computationally demanding. For this reason the following chapter shows some approximations that can be introduced in order to reduce this computational demand, reaching eventually the Hartree-Fock equations, which will be the starting point for the development of the Khon and Sham formulation of *Density Functional Theory*.

2.1 Many-body Schrödinger equation

At the atomic scale materials are agglomerations of electrons and nuclei, bounded together by the attractive and repulsive forces between them. To describe a quantum system composed by N electrons and M nuclei one will need to introduce a many-body Schrödinger equation: $\Psi = \Psi(\vec{r_1}, ..., \vec{r_N}; \vec{R_1}, ..., \vec{R_M})$, where $\vec{r_i}$, with $i = 1, ..., N$ represent the positions of the electrons, while $\vec{R_I}$, with $I = 1, ..., M$ represent the positions of the nuclei. It is thus possible to obtain the kinetic energy and the potential energies of the system, which will be included in the Schrödinger equation:

- Kinetic energy: $\hat{T} = -\sum_{i=1}^{N} \frac{\hbar^2}{2m_e} \nabla_i^2 - \sum_{I=1}^{M} \frac{\hbar^2}{2M_I} \nabla_I^2$
- Repulsive potential between the electrons: $\hat{V}_{ee} = \frac{1}{2} \sum_{i \neq j} \frac{e^2}{4\pi\epsilon_0} \frac{1}{|\vec{r_i} - \vec{r_j}|}$
- Repulsive potential between the nuclei: $\hat{V}_{nn} = \frac{1}{2} \sum_{I \neq J} \frac{e^2}{4\pi\epsilon_0} \frac{Z_I Z_J}{|\vec{R_I} - \vec{R_J}|}$
- Attractive potential between nuclei and electrons: $\hat{V}_{ne} = -\sum_{i,I} \frac{e^2}{4\pi\epsilon_0} \frac{Z_I}{|\vec{r_i} - \vec{R_I}|}$

where Z_I and Z_J represent the atomic numbers of the different elements which compose the material studied.
Their sum will yield the Hamiltonian of the system, through which one can write the eigenvalue equation of the problem:

$$\hat{H}\Psi = [\hat{T} + \hat{V}_{ee} + \hat{V}_{nn} + \hat{V}_{ne}]\Psi = E_{tot}\Psi \tag{2.1}$$

It is more convenient to write this Hamiltonian using atomic units:

$$\hat{H} = -\sum_i \frac{\nabla_i^2}{2} - \sum_I \frac{\nabla_I^2}{2M_I} + \frac{1}{2}\sum_{i\neq j} \frac{1}{|\vec{r_i} - \vec{r_j}|} + \frac{1}{2}\sum_{I\neq J} \frac{Z_I Z_J}{|\vec{R_I} - \vec{R_J}|} - \sum_{i,I} \frac{Z_I}{|\vec{r_i} - \vec{R_I}|} \tag{2.2}$$

The dimension of this problem can be esteemed even taking into account a system made up of a single iron atom. One can imagine to solve the single body Schrödinger problem for every electron of the system (which is an underestimation of the problem, since correlation is being ignored) and store the wavefunctions in three dimensional arrays with 10 points along each spacial direction. For a single electron one will thus have 10^3 points, and for the iron atom one would have $26 \cdot 10^3$ points. However, in reality, when considering all the 26 electrons of the iron atom, also the interactions and correlations of every electron with all the others need to be included. This means that every electron will provide 3 spatial dimensions to the problem for a total of $10^{3\cdot 26} = 10^{78}$ data points. This is much more than any computer could store.
The aim of *Density Functional Theory* (DFT) will thus be reducing the dimensionality of this problem.

2.1.1 Born-Oppenheimer approximation

One first approximation that can be done in order to simplify the problem is considering that nuclei in a solid material typically remain near certain positions, so that they can be assumed clamped near these positions[1]. This way the masses of the nuclei can be considered $M_I = \infty$, which means that the contribution of the nuclei to the kinetic term can be considered 0 and, since R_I do not change, the potential energy between the nuclei becomes a constant, which can be subtracted to the total energy of the system, in order to obtain an energy E:

$$E = E_{tot} - \frac{1}{2}\sum_{I\neq J} \frac{Z_I Z_J}{|\vec{R_I} - \vec{R_J}|}$$

This way the Hamiltonian 2.2 can be simplified, and the eigenvalue problem becomes:

$$-\sum_i \frac{\nabla_i^2}{2} + \frac{1}{2}\sum_{i\neq j} \frac{1}{|\vec{r_i} - \vec{r_j}|} - \sum_{i,I} \frac{Z_I}{|\vec{r_i} - \vec{R_I}|} = E\Psi \tag{2.3}$$

It can thus be noticed that the last term of the Hamiltonian represent the sum of the Coulomb potentials experienced by every single electron:

$$\hat{V}_n(\vec{r}) = -\sum_I \frac{Z_I}{|\vec{r} - \vec{R_I}|}$$

The Hamiltonian of this system can be separated in the sum of the potential energy due to the interactions between the electrons and the sum of N single electrons Hamiltonians H_0:

$$\hat{H_0}(\vec{r_i}) = -\frac{\nabla_i^2}{2} - \hat{V}_n(\vec{r_i}) \tag{2.4}$$

so that the Hamiltonian can be written as:

[1]The uncertainty principle actually prevents nuclei from being perfectly immobile, since the uncertainties in momentum and position must satisfy: $\Delta p_x \Delta x \geq \hbar$

$$\hat{H}(\vec{r_1}, ..., \vec{r_N}) = \sum_i \hat{H}_0(\vec{r_i}) + \frac{1}{2} \sum_{i \neq j} \frac{1}{|\vec{r_i} - \vec{r_j}|} \tag{2.5}$$

Since the nuclei are now clamped, $\hat{H}$, and thus also Ψ, are now functions only of the positions of the electrons. This approximation, that allowed to treat nuclei and electrons separately, is known as *Born-Oppenheimer approximation.*

2.1.2 Independent electrons approximation

A first approximation in order to obtain the wavefunction Ψ is to consider the electrons independent from each other and thus ignoring the last term in the Hamiltonian 2.5, which will reduce the problem to

$$\sum_i \hat{H}_0(\vec{r_i})\Psi = E\Psi = \sum_i \epsilon_i \Psi$$

for which the wavefunction Ψ is given by the product of N single electron wavefunctions $\phi_i(\vec{r_i})$:

$$\Psi(\vec{r_1}, ..., \vec{r_N}) = \phi_1(\vec{r_1})\phi_2(r_2)...\phi_N(\vec{r_N})$$

Each of the ϕ_i solves the single body Schrödinger problem:

$$\hat{H}_0(r_i)\phi_i(\vec{r_i}) = \epsilon_i \phi_i(\vec{r_i})$$

and the total energy E of the system is given by the sum of the energies ϵ_i of these Schrödinger problems.

This approximation leads to inaccurate results, since the interaction between electrons and the effects of Pauli exclusion principle are not negligible compared to the other terms in the equation, but it is a good starting point because of its simplicity and will later be modified in order to improve results.

2.1.3 Mean field approximation

Taking into account the interaction between the electrons, one can consider every single electron experiencing a potential field V_H (Hartree potential) which represent the mean potential field generated by the charge distribution of all the other electrons. From classical electrostatic *Poisson's equation* must hold:

$$\nabla^2 V_H(\vec{r}) = -4\pi n(\vec{r})$$

where $n(\vec{r})$ is the electronic charge density, which can be expressed as the probability of finding any electron at position $\vec{r}$ and for independent electrons can be expressed as:

$$n(\vec{r}) = \sum_j |\phi_j(\vec{r})|^2 \tag{2.6}$$

The formal solution of *Poisson's equation* gives the potential acting on every electron:

$$V_H(\vec{r_i}) = \int d\vec{r_j} \frac{n(\vec{r_j})}{|\vec{r_j} - \vec{r_i}|} = \sum_{j \neq i} \int d\vec{r_j} \frac{|\phi_j(\vec{r_j})|^2}{|\vec{r_j} - \vec{r_i}|} \tag{2.7}$$

2.2 Hartree-Fock equations

2.2.1 The variational principle

Assuming to know the exact many-body wavefunction $\Psi(\vec{r_1}, ..., \vec{r_n})$ the energy of the ground sate of the system can be obtained as:

$$E[\Psi] = \frac{\langle\Psi|\,\hat{H}\,|\Psi\rangle}{\langle\Psi|\Psi\rangle}$$

where $E[\Psi]$ is a functional. For a generic wavefunction, different from the exact one, the formula still holds, but it will not yield anymore the ground-state energy E_0, but an energy $E[\Psi] \geq E_0$. This means that one can choose the parameters in order to minimize this functional, so, combining this variational principle with the hypothesis of independent electrons, the minimum condition is given by the functional derivative:

$$\frac{\delta\,\langle\Psi|\,\hat{H}\,|\Psi\rangle}{\delta\phi_i} = \frac{\delta E}{\delta\phi_i} = 0 \tag{2.8}$$

This derivative can be computed taking into account that the ϕ_i must be orthonormal, which acts as a constrain and the procedure leads to N integro-differential equations, the Hartree equations:

$$\left[-\frac{1}{2}\nabla_i^2 + \hat{V}_n(\vec{r_i}) + \hat{V}_H(\vec{r_i})\right]\phi_i(\vec{r_i}) = \epsilon_i\phi_i(\vec{r_i})$$

This equation is self consistent; indeed, the Hartree term 2.7 explicitly depends on the orbitals ϕ_j, which are the solutions of the other Hartree equations.
A typical strategy to solve this system of equations consist in an iterative solution. An initial guess is chosen for the orbital in order to construct the Hartree operator and solve the single particle Hartree equations. This solutions are then used again to construct the Hartree operator and the procedure is repeated till convergence is reached.

2.2.2 Slater determinant and exchange term

The wavefunction Ψ considered so far, however, does not include nor the effects of the exchange of the electrons nor their correlation. Indeed, due to the fermionic nature of electrons, Ψ must be anti-symmetric with respect to particles exchange:

$$\Psi(\vec{r_1}, ..., \vec{r_i}, ..., \vec{r_j}, ..., \vec{r_N}) = -\Psi(\vec{r_1}, ..., \vec{r_j}, ..., \vec{r_i}, ..., \vec{r_N})$$

In order to include the effect of this exchange, Fock expressed the wavefunction as a *Slater determinant* of the single electron wavefunctions:

$$\Psi = \frac{1}{\sqrt{n!}}\begin{vmatrix} \phi_1(\vec{r_1}) & \phi_2(\vec{r_1}) & ... & \phi_N(\vec{r_1}) \\ \phi_1(\vec{r_2}) & \phi_2(\vec{r_2}) & ... & \phi_N(\vec{r_2}) \\ ... & ... & ... & ... \\ \phi_1(\vec{r_N}) & \phi_2(\vec{r_N}) & ... & \phi_N(\vec{r_N}) \end{vmatrix}$$

which satisfies the Pauli principle due the properties of the determinant of a matrix (notice that, despite this, correlation is still being ignored).
Using wavefunctions given by a Slater determinant in variational principle 2.8 the new set of differential equations becomes:

$$\left[\frac{1}{2}\nabla_i^2 + V_n(\vec{r})\right]\phi_i(\vec{r_i}) + \left[\sum_j \int \phi_j^*(\vec{r_j})\frac{1}{|\vec{r_j}-\vec{r_i}|}\phi_j(\vec{r_j})d\vec{r_j}\right]\phi_i(\vec{r_i}) + \sum_j \left[\int \phi_j^*(\vec{r_j})\frac{1}{|\vec{r_j}-\vec{r_i}|}\phi_i(\vec{r_j})d\vec{r_j}\right]\phi_j(\vec{r_i}) = \epsilon\phi_i(\vec{r_i}) \tag{2.9}$$

where the second term is still an Hartree term with similar meaning to the one in equation 2.7, but where the sum is extended to all electrons, so that each one of them experiences a Coulomb interaction also with itself ($i = j$). This self interaction will be removed from the new term which comes out in this equation, the exchange potential, which comes from purely quantum-mechanical properties of particles.

With an experimental measurement one can obtain the exact value of the energy E_{exact}, which will in general be smaller than the energy obtained with the Hartree-Fock method, since correlations are being ignored so far: $E_{HF} \geq E_{exact}$. By definition the difference between these two energies is called correlation energy:

$$E_{correlation} = E_{HF} - E_{exact}$$

2.3 Kohn-Sham equation

Eq. 2.9 can be written in a simpler form as ([14], pg. 35):

$$\left[-\frac{\nabla_i^2}{2} + \hat{V}_n(\vec{r_i}) + \hat{V}_H(\vec{r_i}) + \hat{V}_X(\vec{r_i})\right]\phi_i(\vec{r_i}) = \epsilon_i\phi_i(\vec{r_i}) \tag{2.10}$$

where V_X represents the exchange term obtained previously. This equation still ignores correlation between electrons. In order to understand how this correlation works one can consider a space region where the probability of finding an electron is high. This means that the probability of finding another electron in the same space region is reduced because of Coulombian repulsion, which means that $|\Psi(\vec{r_1},\vec{r_2})|^2 < |\phi_1(\vec{r_1})\phi_2(\vec{r_2})|^2$ for a system of two electrons. In order to include correlation another term can be added to eq. 2.10: the correlation term $\hat{V}_c$. Eq 2.10 then becomes:

$$\left[-\frac{\nabla_i^2}{2} + \hat{V}_n(\vec{r_i}) + \hat{V}_H(\vec{r_i}) + \hat{V}_X(\vec{r_i}) + \hat{V}_c(\vec{r_i})\right]\phi_i(\vec{r_i}) = \epsilon_i\phi_i(\vec{r_i}) \tag{2.11}$$

An equation of this form is called *Kohn-Sham equation*. Today the exact form of the potential V_c is still not known, but convenient approximations have been developed.

Chapter 3

Density Functional Theory

The Hartree Fock method exposed in the previous chapter considers the energy of the ground state as a functional of the wavefunction Ψ, which means that it depends on the dimension of the $\hat{H}$ considered and could diverge in some situations. It is thus useful considering some global properties of the wavefunction, in order to reduce the dimensionality of the problem. The one introduced in this chapter is the electronic charge density, which is the starting point for developing *Density Functional Theory* (DFT), which will be the main topic of this chapter.

3.1 Electronic charge density

As stated in section 2.1.3 the electronic charge density $n(\vec{r})$ represents the probability of finding an electron at position $\vec{r}$. In quantum mechanic the probability of finding an electron of a system labelled by i at position $\vec{r}$ is given by:

$$P(\vec{r_i} = \vec{r}) = \int |\Psi(\vec{r_1}, ...\vec{r_{i-1}}, \vec{r}, \vec{r_{i+1}}, ...\vec{r_N})|^2 d\vec{r_1}...d\vec{r_{i-1}}d\vec{r_{i+1}}...d\vec{r_N}$$

The electronic charge density will thus be given by:

$$n(\vec{r}) = P(\vec{r_1} = \vec{r}) + ... + P(\vec{r_N} = \vec{r})$$

and since electrons are indistinguishable particles: $P(\vec{r_i} = \vec{r}) = P(\vec{r_j} = \vec{r})\ \forall\ i, j \in [1, ..., N]$, which leads to:

$$n(\vec{r}) = N \int |\Psi(\vec{r}, \vec{r_2}, ...\vec{r_N})|^2 d\vec{r_2}...d\vec{r_N}$$

where N represents the number of electrons in the system. Since $n(\vec{r})$ is the electronic charge density its integral must give the total number of electrons:

$$\int n(\vec{r}) d\vec{r} = N \tag{3.1}$$

Moving from the wavefunction $\Psi(\vec{r_1}, ..., \vec{r_N})$ to the density $n(\vec{r})$ reduces the dimensionality of the problem, since the wavefunction is a function of $3N$ variables, the three components of the position vector for each of the N electrons of the system, while the charge density is a function of only 3 variables.

3.2 Hohenberg-Kohn theorems

The "shape" of the Schrödinger equation is given by the external potential V and the number of electrons N. The aim of the two Hohenberg-Kohn theorems is to relate these quantities.

Theorem 1. *The external potential of a system of interacting electrons is a unique functional of the electronic charge density of the ground state $n(\vec{r})$.*

Proof. Supposing two different potentials V and $\tilde{V}$ exist, with respective ground states Ψ and $\tilde{\Psi}$, both of them will have to lead to the same charge density $n(\vec{r})$. Assuming these ground states have non degenerate energies E and $\tilde{E}$ one can take $\tilde{\Psi}$ as the trial solution for the Hamiltonian $\hat{H}$ of the system with ground state Ψ and, consequently, for the energy E of the ground state Ψ, must hold:

$$E < \langle\tilde{\Psi}|\,\hat{H}\,|\tilde{\Psi}\rangle = \langle\tilde{\Psi}|\,\hat{H} + \hat{\tilde{H}} - \hat{\tilde{H}}\,|\tilde{\Psi}\rangle = \langle\tilde{\Psi}|\,\hat{\tilde{H}}\,|\tilde{\Psi}\rangle + \langle\tilde{\Psi}|\,\hat{H} - \hat{\tilde{H}}\,|\tilde{\Psi}\rangle$$

The first term is the ground state energy $\tilde{E}$, while, for the second one, the kinetic term of both $\hat{H}$ and $\hat{\tilde{H}}$ is the same, since they represent the same system, which means that the difference between the two Hamiltonians is the difference between the two potential terms. Remembering then, that $\tilde{\Psi}^*\tilde{\Psi} = \Psi^*\Psi = n(\vec{r})$:

$$E < \tilde{E} + \int n(\vec{r})\left[V(\vec{r}) - \tilde{V}(\vec{r})\right] d\vec{r}$$

with the consequent result:

$$E - \tilde{E} < \int n(\vec{r})\left[V(\vec{r}) - \tilde{V}(\vec{r})\right] d\vec{r}$$

The same procedure can be followed in order to find the expectation value of Ψ with respect to $\hat{\tilde{H}}$ and considering $\tilde{E}$ as the ground state energy of $\hat{\tilde{H}}$, leading to the result:

$$E - \tilde{E} > \int n(\vec{r})\left[V(\vec{r}) - \tilde{V}(\vec{r})\right] d\vec{r}$$

This result is, obviously, a contradiction, which means that the two potentials V and $\tilde{V}$ can not be different, and thus implying a biunivocal correlation between $n(\vec{r})$ and the external potential $V_{ext}(\vec{r})$.

□

Consequently the non degenerate energy of the ground state is a functional of the charge density of the ground state $n_0(\vec{r})$ only: $E_0 = \langle\Psi_0|\,\hat{H}\,|\Psi_0\rangle = E_0[n_0(\vec{r})]$. This means that the same property will hold for the different components of the energy (which come from the different terms of the Hamiltonian):

$$E_0[n_0(\vec{r})] = T[n_0(\vec{r})] + E_{ee}[n_0(\vec{r})] + E_{ext}[n_0(\vec{r})]$$

where the last term E_{ext} is specific of the problem and could be, for example, the electrons-nuclei interaction, while the first two terms are a universal part and do not depend on the specific problem studied. This universal part can be collected in a functional known as the Hohenberg-Kohn functional:

$$F_{HK}[n_0(\vec{r})] = T[n_0(\vec{r})] + E_{ee}[n_0(\vec{r})] = \langle\Psi_0|\,\hat{T} + \hat{V}_{ee}\,|\Psi_0\rangle \tag{3.2}$$

This leads to the final expression for the energy of the ground state:

$$E_0[n_0(\vec{r})] = \int n_0(\vec{r})V_{ext}(\vec{r})d\vec{r} + F_{HK}[n_0(\vec{r})]$$

The functional $F_{HK}[n]$ could thus be used in order to find the exact solution of the Schrödinger problem, and being universal it would also be system independent. However the form of this functional in unknown, since it would require to be able to introduce exchange and correlation properties. Despite this, useful approximations have been developed, using, for example, the homogeneous electron gas model, for which these properties are known, as local approximation.

The next step is to determine a way to obtain $n_0(\vec{r})$ and E_0, which is the aim of the second Hohenberg-Kohn theorem:

Theorem 2. *If the energy $E_0[n(\vec{r})]$ of a certain ground state $|\Psi_0\rangle$ is non-degenerate and can be expressed as a functional of a density $n(\vec{r})$, then the real density $n_0(\vec{r})$ of the system is the one that minimizes the energy functional E_0, and consequently: $E_0[n(\vec{r})] \geq E_0[n_0(\vec{r})]$.*

Proof. Since for the first Hohenberg-Kohn theorem the external potential is uniquely specified by the charge density $n_0(\vec{r})$ any other charge density $n(\vec{r})$ will be related to a different potential, and will thus correspond the a ground state $|\Psi\rangle$ of a different Hamiltonian, which will be different from the ground state $|\Psi_0\rangle$ of the considered Hamiltonian $\hat{H}$:

$$E_0[n(\vec{r})] = \langle\Psi|\,\hat{H}\,|\Psi\rangle \geq \langle\Psi_0|\,\hat{H}\,|\Psi_0\rangle = E_0[n_0(\vec{r})]$$

□

Taking into account that the number N of electrons in the system is a constrain (eq. 3.1) the minimization problem can be written using Lagrange multipliers as:

$$\frac{\delta\left[E_0[n(\vec{r})] - \mu\left(\int d\vec{r}n(\vec{r}) - N\right)\right]}{\delta n(\vec{r})} = 0$$

where μ (the Lagrange multiplier) is the chemical potential, since the ground state is considered at $T = 0K$.

Using functional 3.2 the second theorem can be written as:

$$\langle\Psi|\,\hat{H}\,|\Psi\rangle = \langle\Psi|\,\hat{T} + \hat{V}_{ee} + \hat{V}_{ext}\,|\Psi\rangle = F_{HK}[n(\vec{r})] + \int V_{ext}(\vec{r})n(\vec{r})d\vec{r} \geq E_0$$

However these theorems only guarantee the uniqueness of such functional, but there is no way to know if a certain density can be obtained from an Hamiltonian with a suitable external potential. In such cases the density is said to be *"V-representable"*.

3.3 Kohn-Sham equations

The starting point of the procedure developed by Kohn and Sham is based on the assumption of the Hartree-Fock problem and thus considers a ground state built from a Slater determinant, which means that the electrons are considered non-interacting. Such electrons are embedded in an effective external potential which ensures that their ground state charge density is the same of the equivalent interacting system.
The ground state $|\Psi_0\rangle$ of the system can be expressed as the Slater determinant of the orthonormal single particle states $\psi_i(\vec{r},\sigma)$, where σ represents the spin dependence of the wavefunctions. With these states, the electronic charge density for the non interacting system is given by 2.6:

$$n(\vec{r}) = \sum_{i,\sigma} |\psi_i(\vec{r},\sigma)|^2 \tag{3.3}$$

Considering now functional 3.2 the kinetic term for a non interacting system is well defined as a functional of n[1] and is the sum of the kinetic energies of the single particles. For what concerns the energy due to the interaction between electrons, also the Hartree term is well defined since, from 2.7:

$$E_H[n(\vec{r})] = \frac{1}{2}\int n(\vec{r})V_H(\vec{r})d\vec{r} = \frac{1}{2}\int\int \frac{n(\vec{r})n(\vec{r'})}{|\vec{r}-\vec{r'}|}d\vec{r}d\vec{r'} \tag{3.4}$$

where the 1/2 factor is added in order to avoid double counting, since the two charge densities implies two sums on the same indexes from eq. 3.3.

Everything that is still unknown (the exchange and correlation terms) is put together in an only term, the *exchange-correlation energy*:

$$F[n(\vec{r})] = T[n(\vec{r})] + E_H[n(\vec{r})] + E_{xc}[n(\vec{r})]$$

The total energy of the ground state $|\Psi_0\rangle$ of the system, considering it expressed as the Slater determinant of the ψ_i, can thus be expressed as:

$$\begin{aligned} &E[n(\vec{r})] = \langle\Psi_0|\,\hat{H}\,|\Psi_0\rangle = \\ &= \sum_{i,\sigma}\left[-\frac{1}{2}\int \psi_i^*(\vec{r},\sigma)\nabla^2\psi_i(\vec{r},\sigma)d\vec{r}\right] + E_H[n(\vec{r})] + E_{xc}[n(\vec{r})] + \int V_{ext}(\vec{r})n(\vec{r})d\vec{r} \end{aligned} \tag{3.5}$$

The minimization of the previous functional with respect to the $\psi_i(\vec{r},\sigma)$ with the constrain that the $\psi_i(\vec{r},\sigma)$ must be normalized leads to the equations:

$$\hat{H}_{KS}\psi_i(\vec{r},\sigma) = \epsilon_{i,\sigma}\psi_i(\vec{r},\sigma) \tag{3.6}$$

where:

$$\hat{H}_{KS} = -\frac{1}{2}\nabla^2 + \hat{V}_H(\vec{r}) + \hat{V}_{xc}(\vec{r}) + \hat{V}_{ext}(\vec{r}) \tag{3.7}$$

which are equations of the form 2.11 and are thus *Kohn-Sham equations*. In this last one $V_{xc}(\vec{r})$ is called *exchange and correlation potential* and is given by:

[1] This kinetic energy represents the energy of the non-interacting system, which is, in general, different from the one of the exact ground state wavefunction.

$$V_{xc}(\vec{r}) = \left.\frac{\delta E_{xc}[n]}{\delta n}\right|_{n(\vec{r})}$$

Equations 3.6 imply that it must exist a functional $E_{xc}[n(\vec{r})]$ which, through a self consistent calculation, allows to obtain the energy of the ground state of the system. However the expression of this functional is not known, but some useful approximations can be used in order to obtain significant results.

3.4 Local Density Approximation

The *Local Density Approximation (LDA)* allows to obtain an approximation of the *exchange and correlation energy* using the simple model of the *Homogeneous Electron Gas*, where the potential of the nuclei and the charge density $n(\vec{r})$ are assumed to be constant [14] [15].
For this model the charge density is known and is equal to: $n = k_F^3/3\pi^2$ ([14], pg. 41), where k_F is the modulus of the Fermi wavevector, which corresponds to the one for which: $E_F = \hbar^2 k_F^2/2m$. It is then possible to obtain an expression for the exchange and correlation energy.
The charge density of the system can be considered as the density of an homogeneous electron gas in the nearby of every point and thus, at every point, the exchange and correlation energy can be constructed using the one of the electron gas.
This way the meaningful property that is interesting to compute is the energy over the volume unit considered: $\epsilon^{HEG}[n] = E^{HEG}[n]/V$. This energy density can then be decomposed in a kinetic part, an exchange part and a correlation part:

$$\epsilon^{HEG} = \epsilon_{kin}^{HEG} + \epsilon_x^{HEG} + \epsilon_c^{HEG}$$

where the kinetic and exchange terms are known:

$$\epsilon_{kin}^{HEG} = \frac{(3\pi^2 n)^{5/3}}{10\pi^2} \qquad \epsilon_x^{HEG} = \frac{(3\pi^2 n)^{4/3}}{4\pi^3}$$

while the correlation term does not have an analytical form, but can be obtained with stochastic numerical methods ([14], pg. 43).
Eventually the *exchange and correlation energy* can be obtained integrating the energy density of the homogeneous electron gas evaluated at the density at each point $\vec{r}$ over the entire system:

$$E_{xc}^{LDA} = \int d\vec{r} \epsilon_{xc}^{HEG}[n(\vec{r})]$$

where $\epsilon_{xc}^{HEG} = \epsilon_x^{HEG} + \epsilon_c^{HEG}$.
This approximation is fairly good for several applications, but can be inaccurate for some chemical applications.

In order to overcome some of the inaccuracies of this theory an improvement that can be done is considering the exchange and correlation energy density not only as a functional of $n(\vec{r})$ at a specific point in space, but also of its gradient at that point:

$$E_{xc}^{GGA} = \int d\vec{r} \epsilon_{xc}[n(\vec{r}), \nabla n(\vec{r})]$$

This approximation is known as *General Gradient Approximation (GGA)* [14] [15].

3.5 Self consistent calculations

3.5.1 The eigenvalue problem

In DFT calculations the aim is to solve a Schrödinger problem of the form $\hat{H}|\psi\rangle = E|\psi\rangle$,where, in the Kohn and Sham formulation, the Hamiltonian is given by 3.7 and the Hartree term and the exchange and correlation term introduce non-linear parts in the problem.
The starting point is to expand the wavefunction in a basis:

$$|\psi\rangle = \sum_{i=1}^{N} c_i |\phi_i\rangle \tag{3.8}$$

where the coefficients c_i, can be, in general, complex numbers and N can also be infinite.
Projecting now the eigenvalue equation on each basis element:

$$\langle\phi_i| \hat{H} |\psi\rangle = E \langle\phi_i|\psi\rangle$$

Using now expansion 3.8 for the wavefunction:

$$\sum_j c_j \langle\phi_i| \hat{H} |\phi_j\rangle = E \sum_j c_j \langle\phi_i|\phi_j\rangle = E \sum_j c_j \delta_{ij} = E c_i$$

The left hand side of the equation represents the matrix elements of the Hamiltonian H_{ij}, so that the problem can be written, using *Einstein notation*, as:

$$H_{ij} c_j = E \delta_{ij} c_j$$

leading to an equation of the form:

$$(H_{ij} - E\delta_{ij}) c_j = 0$$

This is a linear algebra problem where the solution for the eigenvalues E can be obtained from the condition:

$$\det(H_{ij} - E\delta_{ij}) = 0$$

which leads to an N^{th} degree polynomial equation, whose N solutions will be the energy eigenvalues.
The goal is now finding a good basis in order to expand the wavefunction as in eq. 3.8.

3.5.2 The iterative procedure

It has been shown that equations 3.6 can be reduced to eigenvalue problems, whose solutions lead to the eigenvalues $\epsilon_{i,\sigma}$ and the eigenfunctions ψ_i of the single particles problems. In order to solve these problems one need to know all the potential terms in Hamiltonian 3.7. The complication here is that $\hat{V}_H$ and $\hat{V}_{xc}$ depend on the charge density n, which depends itself on the unknown eigenfunctions as in equation 3.3. This means that every solution ψ_i depends on all the other solutions ψ_j, which makes the problem *self-consistent*.

The practical procedure for solving the *Kohn-Sham equations* consists in:

1. Specifying the nuclei coordinates in order to obtain the external potential (this information is typically available from crystallography data);
2. Choosing a starting guess of the electronic density $n(\vec{r})$ in order to obtain $\hat{V}_H$ and $\hat{V}_{xc}$. A useful starting approximation consists in considering it as the sum of the densities of completely isolated atoms arranged in the atomic positions of the material considered;
3. Estimating the total potential and proceed to the numeric solution of the *Kohn-Sham equations*;
4. Constructing a better density with the new eigenfunctions;
5. Using the new density instead of the previous guess in point 2 and repeating the procedure.

This series of steps is followed till the density obtained in step 4 matches the one used in step 2 within a certain specified convergence criteria.

With the density just obtained it is possible to calculate the total energy of the system from equation 3.5. This ground state total energy can then be used in order to calculate many properties of the material.

3.6 Applications of DFT

3.6.1 Equilibrium structure for materials

One important assumption made in section 2.1.1 is that the positions of the nuclei do not change. This is true when the total force acting on them vanishes, which means that, for a given structure, it is important to be able to calculate the total force acting on the nuclei and find the nuclear coordinates for which these forces are identically zero.
Reintroducing the nuclei motion means that the starting point of this theory will, again, be equation 2.1 and the eigenfunctions will depend on both the electrons and nuclei positions.
A first useful approximation comes from the consideration that the potential felt by an electron in the middle of an interatomic bond or by a nucleus around its equilibrium position can be approximated as the one of an harmonic oscillator. This means that their wavefunctions can be approximated by those of the harmonic oscillator, which, for the ground state, are Gaussians with standard deviations that scales with the particles masses as: $\sigma \sim M^{-1/4}$. This means that the wavefunction of the electrons is much more spreaded in space than the nuclei one and, consequently, the motion of the nuclei will be much smaller that the one of the electrons and one could first determine the electrons wavefunction for a set of fixed nuclear positions, and then allow the nuclei to move according to their quantum-mechanical wavefunction, which will not change much and thus not affect too much the electronic wavefunction.
The formal consequence of this effect is that the wavefunction of both the electrons and nuclei positions can be separated into the product of two wavefunctions, each of which will depend only on one of the two sets of coordinates:

$$\Psi(\vec{r_1}, ..., \vec{r_N}, \vec{R_1}, ..., \vec{R_M}) = \psi^{(e)}_{\vec{R}}(\vec{r_1}, ..., \vec{r_N})\psi^{(n)}(\vec{R_1}, ..., \vec{R_M})$$

where the electronic part depends parametrically on the set of nuclei positions. Since the electrons and the nuclei are now being treated separately this approximation is still a *Born-Oppenheimer approximation*, as the one introduced in section 2.1.1.
This way, for the electronic wavefunction, a Schrödinger equation of the form 2.3 will still hold, which means that equation 2.1 can be rewritten as:

$$E\psi^{(e)}_{\vec{R}}\psi^{(n)} + \left[-\sum_I \frac{\nabla_I^2}{2M_I} + \frac{1}{2}\sum_{I\neq J}\frac{Z_I Z_J}{|\vec{R_I}-\vec{R_J}|}\right]\psi^{(e)}_{\vec{R}}\psi^{(n)} = E_{tot}\psi^{(e)}_{\vec{R}}\psi^{(n)}$$

finally, multiplying both sides by the complex conjugate of $\psi^e_{\vec{R}}$, integrating over the positions of the electrons and taking into account that the total wavefunction Ψ must be normalized, this equation becomes [14]:

$$\left[-\sum_I \frac{\nabla_I^2}{2M_I} + \frac{1}{2}\sum_{I\neq J}\frac{Z_I Z_J}{|\vec{R_I}-\vec{R_J}|} + E(\vec{R_1},...,\vec{R_M})\right]\psi^{(n)} = E_{tot}\psi^{(n)} \tag{3.9}$$

where the electronic contribution is all included in the energy $E(\vec{R_1},...,\vec{R_M})$, which depends on the positions of the nuclei and acts as an effective potential on them.
An important assumption that is being considered in this procedure is that when the nuclear coordinates change the electrons evolve from the ground state associated with the initial configuration to the one of the final configuration, which means that nuclei moves so slowly that electrons have enough time to adjust their positions in order to remain in their lower energy state. As a consequence of this assumption electrons are not exchanging energy with the nuclei and the evolution of the system is *adiabatic*, indeed, this approximation that allowed to separate the electronic part of the wavefunction from the nuclear one, is also called *Adiabatic approximation.*

From eq. 3.9 the Hamiltonian acting on the nuclei is of the form:

$$\hat{H}^{(n)} = -\sum_I \frac{\nabla_I^2}{2M_I} + \hat{U}(\vec{R_1},...,\vec{R_M})$$

where the total potential U is given by the sum of the one due to the interaction between the nuclei and the total energy of the electrons.
As it has been stated before, given the same energy profile, the nuclear wavefunction is much more compact than the electronic one, which means that in comparison with the electrons, nuclei can be considered as point like particles, and thus obey the laws of classical mechanic as a first approximation.
From the classical Hamiltonian dependent on the set of conjugate canonical variables $(\vec{R_I},\vec{P_I})$, with $I = 1,...,M$, one can obtain the force acting on each nucleus starting from the second law of Newton:

$$\begin{aligned}\vec{F_I} = M_I\ddot{\vec{R}}_I = M_I\frac{d}{dt}\dot{\vec{R}}_I = M_I\frac{d}{dt}\frac{\partial H^{(n)}}{\partial\vec{P_I}} = M_I\frac{d}{dt}\frac{\partial}{\partial\vec{P_I}}\left[\sum_J\frac{\vec{P_J}^{\,2}}{2M_J} + U(\vec{R_1},...,\vec{R_M})\right] = \\ = M_I\frac{d}{dt}\frac{\vec{P_I}}{M_I} = \dot{\vec{P}}_I = -\frac{\partial H^{(n)}}{\partial\vec{R_I}} = -\frac{\partial U}{\partial\vec{R_I}}\end{aligned} \tag{3.10}$$

where the canonical relations $\dot{\vec{R}}_I = \partial H^{(n)}/\partial \vec{P}_I$ and $\dot{\vec{P}}_I = -\partial H^{(n)}/\partial \vec{R}_I$ have been used. This result shows that equilibrium structures correspond to stationary points of the function $U(\vec{R}_1, .., \vec{R}_M)$.
Note that all these considerations hold for materials at $T = 0K$, but in many cases the structural properties at ambient temperature are the same as those at $T = 0K$.
However the minimization of the potential energy U with respect to the $3M$ degrees of freedom would be too computationally expensive. It is thus useful taking into account the following *Hellmann-Feynman theorem*:

Theorem. *Given a system described by an Hamiltonian which depends on a parameter λ (in this case λ is the internuclear separation) and whose eigenvalue with respect to its normalized eigenstate $|\psi_\lambda\rangle$ is E_λ:*

$$\frac{\partial E_\lambda}{\partial \lambda} = \left\langle \psi_\lambda \middle| \frac{\partial \hat{H}_\lambda}{\partial \lambda} \middle| \psi_\lambda \right\rangle$$

Proof. The proof follows considering the Leibniz rule and that $\hat{H}_\lambda |\psi_\lambda\rangle = E_\lambda |\psi_\lambda\rangle$:

$$\frac{\partial E_\lambda}{\partial \lambda} = \frac{\partial}{\partial \lambda} \langle \psi_\lambda | \hat{H}_\lambda | \psi_\lambda \rangle = \left\langle \frac{\partial \psi_\lambda}{\partial \lambda} \middle| \hat{H}_\lambda \middle| \psi_\lambda \right\rangle + \left\langle \psi_\lambda \middle| \frac{\partial \hat{H}_\lambda}{\partial \lambda} \middle| \psi_\lambda \right\rangle + \left\langle \psi_\lambda \middle| \hat{H}_\lambda \middle| \frac{\partial \psi_\lambda}{\partial \lambda} \right\rangle =$$

$$= E_\lambda \left\langle \frac{\partial \psi_\lambda}{\partial \lambda} \middle| \psi_\lambda \right\rangle + E_\lambda \left\langle \psi_\lambda \middle| \frac{\partial \psi_\lambda}{\partial \lambda} \right\rangle + \left\langle \psi_\lambda \middle| \frac{\partial \hat{H}_\lambda}{\partial \lambda} \middle| \psi_\lambda \right\rangle =$$

$$= E_\lambda \frac{\partial}{\partial \lambda} \langle \psi_\lambda | \psi_\lambda \rangle + \left\langle \psi_\lambda \middle| \frac{\partial \hat{H}_\lambda}{\partial \lambda} \middle| \psi_\lambda \right\rangle = E_\lambda \frac{\partial}{\partial \lambda} 1 + \left\langle \psi_\lambda \middle| \frac{\partial \hat{H}_\lambda}{\partial \lambda} \middle| \psi_\lambda \right\rangle =$$

$$= \left\langle \psi_\lambda \middle| \frac{\partial \hat{H}_\lambda}{\partial \lambda} \middle| \psi_\lambda \right\rangle$$

□

This allows to pass from $3M$ parameters to only one parameter, reducing drastically the complexity of the problem.
From this the calculation of the forces for all the nuclei in the system can be performed using the electron density of one set of nuclear coordinates, which can be obtained using DFT.
This method allows to research the minimum of the potential energy surface $U(\vec{R}_1, ..., \vec{R}_M)$. A particle left free to move in a position different from the equilibrium position will end up oscillating around a minimum. The effect to reproduce in order to lead the particle on the minimum is the same one that would be included by the friction term proportional to the velocity of the particle in the equation to describe the motion of a body in a viscous fluid.
Practically, after finding the charge density and the total energy with DFT and the total force acting on the system for a given nuclear configuration using *Hellmann-Feynman theorem*, eq. 3.10 with the addition of the friction term is solved numerically discretizing the time variable and approximating the time derivatives with finite differences formulas (*Verlet's algorithm*), leading to an equation that can be used in order to express the new positions as functions of the previous ones. This procedure is then repeated with the new positions found, leading to a series of configurations that will converge to the minimum of the potential surface.

3.6.2 Band structures

Band structures allow to give an interpretation to the eigenvalues of the *Kohn-Sham equations*.
Starting from eq. 3.5 and substituting expression 3.3 for the charge density yields (ignoring the spin dependence) the result:

$$E = \sum_i f_i \int d\vec{r} \psi_i^*(\vec{r}) \left[-\frac{\nabla^2}{2} + V_{ext}(\vec{r}) + \frac{1}{2} \int d\vec{r'} \frac{n(\vec{r'})}{|\vec{r} - \vec{r'}|} \right] \psi_i(\vec{r}) + E_{xc}[n]$$

where f_i is the occupation function and is equal to 1 if state ψ_i is occupied and 0 otherwise.
The integral inside the square brackets corresponds to the *Hartree potential* from equation 2.7 and adding and subtracting $V_H/2 + V_{xc}$ allows to reconstruct the total potential $V_{tot} = V_H + V_{xc} + V_{ext}$:

$$E = \sum_i f_i \int \psi_i^*(\vec{r}) \left[-\frac{\nabla^2}{2} + V_{tot}(\vec{r}) \right] \psi_i(\vec{r}) - \int d\vec{r} n(\vec{r}) \left[\frac{V_H}{2} + V_{xc} \right] + E_{xc}[n]$$

The first integral is equivalent to $\langle \psi_i | \hat{H}_{KS} | \psi_i \rangle$ and from equation 3.6 yields the Kohn and Sham eigenvalues while in the second term the integral of the Hartree potential yields the Hartree energy from equation 3.4, leading to the final expression:

$$E = \sum_i f_i \epsilon_i - \left[E_H + \int d\vec{r} V_{xc} n(\vec{r}) - E_{xc}[n] \right] \tag{3.11}$$

The first term on the left on the right side of this equation is the sum of the energies of all the occupied states and is referred as *band structure energy* while the second one is needed in order to avoid double counting of contributions in the total energy.
Taking the derivative of the total energy with respect to the occupation f_i yields:

$$\frac{\partial E}{\partial f_i} = \epsilon_i$$

From this, one can see that adding an electron to a system of N electrons in a previously unoccupied state ψ_i yields a change in the total energy:

$$E_{N+1,i} - E_N = \int_0^1 df_i \frac{\partial E}{\partial f_i} = \int_0^1 df_i \epsilon_i$$

This means that a change in the occupation f_i will lead to a change in the energy eigenvalue ϵ_i, due to the fact that the new electron will modify the electron density and thus the total potential V_{tot}. However, in a solid, the change in the number of electrons would be so small for a single electron that the change in the charge density can be considered negligible, so, as a first approximation, the eigenvalue ϵ_i can be considered independent from the occupancy f_i:

$$E_{N+1,i} - E_N \simeq \epsilon_i$$

so that the change in the total energy is, approximately, the Kohn-Sham eigenvalue of the new electron and similarly for the removal of an electron. This means that each

electron carries an energy corresponding to the Kohn-Sham eigenvalue of the state that it occupies.

The calculation of the band structure for a crystal starts from *Bloch Theorem* and eq. 1.1, which can be rewritten in this case as:

$$\psi_{i,\vec{k}}(\vec{r}) = e^{i\vec{k}\cdot\vec{r}} u_{i,\vec{k}}(\vec{r}) \tag{3.12}$$

where the parametric dependence of both the wavefunction and u on the wavevector $\vec{k}$ has been marked. Substituting this one in the *Kohn-Sham equation* 3.6 and multiplying both sides by $e^{-i\vec{k}\cdot\vec{r}}$ yields the result:

$$\left[-\frac{1}{2}(\nabla + i\vec{k})^2 + \hat{V}_{tot}\right] u_{i,\vec{k}}(\vec{r}) = \epsilon_{i,\vec{k}} u_{i,\vec{k}}(\vec{r}) \tag{3.13}$$

which is a Schrödinger problem which allows to determine the periodic function $u_{i,\vec{k}}(\vec{r})$, which are considered normalized inside the unit cell of the crystal.
This problem needs to be solved only inside one unit cell, since the solution in any other cell of the crystal can be obtained applying the periodic boundary condition and is identical to the one obtained for the first one. Practically the numerical solution of eq. 3.13 will require the description of $u_{i,\vec{k}}$ on a discrete mesh of points spanning only one unit cell. The periodicity of the crystal allows to restrict the range of wavevectors to consider for the solution to the first *Brillouin Zone*.
The solution of the Kohn and Sham equation in a crystal (eq. 3.13) allows then to construct the electronic charge density using wavefunctions given by 3.12, which will need also an integration over the wavevectors inside the first Brillouin zone:

$$n(\vec{r}) = \sum_i \int_{BZ} \frac{d\vec{k}}{\Omega_{BZ}} f_{i\vec{k}} |u_{i,\vec{k}}(\vec{r})|^2 \tag{3.14}$$

Because of the periodicity of $u_{i,\vec{k}}$ also $n(\vec{r})$ will be the same in every unit cell.
Eq. 3.11 can then be rewritten for the particular case of a crystal solid:

$$E = \sum_i \int_{BZ} \frac{d\vec{k}}{\Omega_{BZ}} f_{i,\vec{k}} \epsilon_{i,\vec{k}} - \left[E_H + \int d\vec{r} V_{xc} n(\vec{r}) - E_{xc}[n]\right] \tag{3.15}$$

considering all quantities as energies per unit cell. The ground state of the system is obtained filling all the electrons states starting from the lowest-energy one, satisfying the constrain that the the charge density integrated over the unit cell must yield the number of electrons per unit cell N. The total energy is minimized when all the states under the Fermi level are occupied and all the above ones are empty.

Practical DFT calculations proceed in a similar way to the one shown in section 3.5.2, but using eq. 3.13 as *Kohn-Sham equations* and eq. 3.14 for the charge density. In this case the integral over the BZ is evaluated numerically by considering a discrete mesh of wavevectors $\vec{k}$ spanning the whole BZ.

Chapter 4

VASP and the implementation of the problem

The *Vienna Ab initio Simulation Package* (VASP) [16] is a program which allows to perform first principles calculations for the properties of materials at the atomic scale following the method explained in the previous chapters and is the one that was used to perform the calculations in this thesis. The following chapter explains how VASP implements some of the details previously explained in order to perform calculations and how its user interface works.

4.1 Plane waves representation

The solution of the Schrödinger problem for a periodic lattice has the form 3.12 and, since $u_{i,\vec{k}}(\vec{r})$ is periodic in space with the same periodicity of the lattice, it can be expanded in terms of a set of plane waves:

$$u_{i,\vec{k}}(\vec{r}) = \sum_{\vec{G}} c_{i,\vec{G}} e^{i\vec{G}\cdot\vec{r}}$$

where $\vec{G}$ is a reciprocal lattice vector defined by:

$$\vec{G} = m_1\vec{b_1} + m_2\vec{b_2} + m_3\vec{b_3}$$

with $\vec{b_1}, \vec{b_2}, \vec{b_3}$ primitive vectors of the reciprocal lattice, and $m_1, m_2, m_3 \in \mathbb{Z}$, which implies an infinite sum over an infinite number of possible values of $\vec{G}$.
This allows to rewrite eq. 3.12 as:

$$\psi_{i,\vec{k}}(\vec{r}) = \sum_{\vec{G}} c_{i,\vec{k}+\vec{G}} e^{i(\vec{k}+\vec{G})\cdot\vec{r}} \tag{4.1}$$

which is a possible basis choice for the expansion 3.8.

Equations of the form 4.1 are solutions of the Schrödinger equation with energy eigenvalues:

$$\epsilon_i = \frac{\hbar^2}{2m}|\vec{k} + \vec{G}|^2$$

Solutions with lower energies are generally more important than solutions with higher energies, which means that the sum can be truncated including only solutions with energies lower than the value:

$$E_{cut} = \frac{\hbar^2}{2m} G_{cut}^2 \tag{4.2}$$

which means that the plane waves considered will be of the form:

$$\psi_{i,\vec{k}}(\vec{r}) \approx \sum_{|\vec{k}+\vec{G}|<G_{cut}} c_{i,\vec{k}+\vec{G}} e^{i(\vec{k}+\vec{G})\cdot\vec{r}} \tag{4.3}$$

The *cutoff value* influences both the precision of the result and the computational time needed for the calculation. For the ENCUT command VASP includes a default cutoff value for each atom, and, if not set, the used one is the highest E_{cut} between those of the atoms considered in the problem.
This plane waves representation is the one used by VASP for the basis 3.8.

4.2 Pseudopotentials

4.2.1 General properties

In molecules and solids not all the electrons are bounded to the nuclei in the same way and the study of different properties does not always require to take into account all the electrons. In particular chemical bonding and other physical characteristics of materials are dominated by the less tightly bounded valence electrons. This fact is a great computational advantage, since, from eq. 4.3, in order to include plane waves that oscillate on short length scales in the real space, such as the one needed for orbitals close to the nucleus, a large energy cutoff would be needed.
The fact that core electrons are not described by the set of plane waves chosen means that their screening effect on the potential of the nucleus felt by the valence electrons must be included through a *pseudopotential*. The pseudopotential must be created in such a way that when valence electrons are placed in its field their energy is exactly the same one they would have had if they felt the full electronic configuration. In addition to this it must be such that the wavefunctions outside the effective core (made by the nucleus and the tight bounded electrons) are the correct ones (Fig. 4.1).

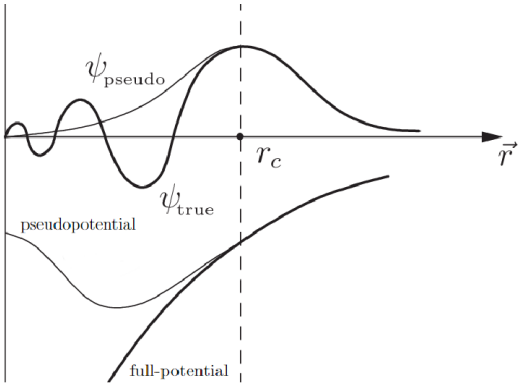

Figure 4.1: *Comparison between the pseudopotential and the real potential and their respective wavefunctions. The effective core radius is denoted by* r_c.

Ideally, a pseudopotential is developed by considering an isolated atom of one element. The resulting pseudopotential can then be used for calculations that place this atom in more complicated structures without adjustments. This desirable property is referred to as the *transferability of the pseudopotential*.

4.2.2 Projected Augmented Wave method

The *Projected Augmented Wave method*, or *PAW method*, used by VASP, considers core electrons fixed at their positions as the nuclei and experiencing a modified potential, while valence electrons are considered subject to a potential which behaves as the real one.
The starting point of the *PAW method* is the *Augmented Plane Wave method (APW)*, where the space is divided into spheres centered on each nucleus site. This spheres do not overlap, so that some space is left free (interstitial region), but almost fill all the allowed space. This implies two different Schrödinger problems: inside the spheres, with a spherically symmetric potential, and in the interstitial region, where the solutions will still be plane waves:

$$\phi_{\vec{G}}(\vec{k},\vec{r}) = \begin{cases} e^{i(\vec{k}+\vec{G})\cdot\vec{r}} & \text{interstitial region} \\ \\ \sum_{l,m} a_{l,m}^{\alpha,\vec{G}}(\vec{k}) u_l(\vec{r_\alpha}, E) Y_{l,m}(\vec{r_\alpha}) & \text{inside the spheres} \end{cases}$$

where u_l satisfies the radial Schrödinger equation, $Y_{l,m}$ are the *spherical harmonics*, α enumerates the spheres, $\vec{r_\alpha}$ is the position inside sphere α with respect to its center and the coefficients $a_{l,m}^{\alpha,\vec{G}}$ are determined requiring that the wavefunctions are continuous at the boundary of the spheres.
With this basis the single particle wavefunctions become:

$$\psi_{i,\vec{k}}(\vec{r}) = \sum_{|\vec{k}+\vec{G}|<G_{cut}} c_{i,\vec{k}}^{\vec{G}} \phi_{\vec{G}}(\vec{k},\vec{r})$$

The augmentation effect is given by the fact that each plane wave, inside the spheres, is augmented by a linear combination of: $u_l(\vec{r_\alpha}, E) Y_{l,m}(\vec{r_\alpha})$.
Negative aspects of this basis are that u_l depends also on the band energy, which leads to a non-linear problem, hard to compute, and that, for some energy values, the spheres boundaries become very small, leading to almost infinite coefficients $a_{l,m}^{\alpha,\vec{G}}$.
To avoid these problems the *Linearized APW method (LAPW)* propose to replace the u_l with their Taylor series truncated to the first order around an energy parameter E_l: $u_l(E) = u_l(E_l) + (E - E_l)\dot{u}_l(E_l) + O(E - E_l)^2$, where the error on the wavefunctions is quadratic in $E - E_l$:

$$\phi_{\vec{G}}(\vec{k},\vec{r}) = \begin{cases} e^{i(\vec{k}+\vec{G})\cdot\vec{r}} \\ \\ \sum_{l,m} [a_{l,m}^{\alpha,\vec{G}}(\vec{k}) u_l(\vec{r_\alpha}, E_l) + b_{l,m}^{\alpha,\vec{G}}(\vec{k})(E - E_l)\dot{u}_l(\vec{r_\alpha}, E_l)] Y_{l,m}(\vec{r_\alpha}) \end{cases}$$

where a and b are still determined with the continuity condition on the boundary of the spheres.

The final improvement is given by the *Full-potential LAPW method*, where a non spherical term inside the spheres is combined with a non constant potential in the interstitial region:

$$V(\vec{r}) = \begin{cases} \sum_{\vec{G}} V_{\vec{G}} e^{i\vec{G}\cdot\vec{r}} & \text{interstitial region} \\ \\ \sum_{l,m} V_{l,m}(r) Y_{l,m}(\vec{r}) & \text{inside the spheres} \end{cases}$$

The *PAW method* is a generalization of the *LAPW method*. The computationally hard part to describe is the one inside the spheres, since there the wavefunctions oscillate very rapidly.
Assuming that $\hat{T}$ is a linear transformation that relates the true Kohn-Sham single particles wavefunctions $|\psi\rangle$ to their "pseudopotential" version $|\tilde{\psi}\rangle$:

$$|\psi\rangle = \hat{T}\,|\tilde{\psi}\rangle$$

With this the expectation value of an observable $\hat{O}$ is given by:

$$\langle\hat{O}\rangle = \langle\psi|\,\hat{O}\,|\psi\rangle = \langle\tilde{\psi}|\,\hat{T}^{\dagger}\hat{O}\hat{T}\,|\tilde{\psi}\rangle = \langle\tilde{\psi}|\,\hat{\tilde{O}}\,|\tilde{\psi}\rangle$$

Since the wavefunctions outside the spheres must agree with the real ones the transformation $\hat{T}$ differs from the identity only for a sum of atom centered contributions:

$$\hat{T} = \hat{\mathbb{1}} + \sum_{\vec{R}} \hat{T}_{\vec{R}} \tag{4.4}$$

where $\hat{T}_{\vec{R}}$ acts on a specific spherical region Ω_R, so that the transformation inside these acts on the basis elements within Ω_R as:

$$|\phi_i\rangle = (\hat{\mathbb{1}} + \hat{T}_{\vec{R}})\,|\tilde{\phi}_i\rangle \tag{4.5}$$

and thus the single particles wavefunctions become:

$$|\psi\rangle = \sum_i c_i\,|\phi_i\rangle = \sum_i c_i(\mathbb{1} + \hat{T}_{\vec{R},i})\,|\tilde{\phi}_i\rangle = \hat{T}\sum_i c_i\,|\tilde{\phi}_i\rangle = \hat{T}\,|\tilde{\psi}_i\rangle$$

where the dependence on i of $\hat{T}_{\vec{R},i}$ specifies which sphere is considered for each ϕ_i in expression 4.5 and allows to obtain expression 4.4 for $\hat{T}$.
Coefficients c_i are the same for both $|\psi\rangle$ and $|\tilde{\psi}\rangle$ and can be obtained using the orthogonal projection functions $\langle p_i|$ and $\langle\tilde{p}_i|$, for which completeness and orthogonality relations hold:

$$c_i = \langle p_i|\psi\rangle = \langle\tilde{p}_i|\tilde{\psi}\rangle$$

With these functions the wavefunctions inside the spheres become:

$$|\tilde{\psi}\rangle = \sum_i |\tilde{\phi}_i\rangle\ \langle\tilde{p}_i|\tilde{\psi}\rangle$$

For the basis wavefunctions inside the spheres hold: $\langle \tilde{p}_i | \tilde{\phi}_j \rangle = \delta_{i,j}$, while the projection of the part of the wavefunction $|\psi\rangle$ outside the spheres is null.
The transformation operator $\hat{T}$ can be written as:

$$\hat{T} = \hat{\mathbb{1}} + \sum_i (|\phi_i\rangle - |\tilde{\phi}_i\rangle) \langle \tilde{p}_i|$$

indeed, applying it to a ket $|\tilde{\psi}\rangle$:

$$\hat{T}|\tilde{\psi}\rangle = \left(\hat{\mathbb{1}} + \sum_i (|\phi_i\rangle - |\tilde{\phi}_i\rangle) \langle \tilde{p}_i|\right) \left(\sum_j c_j |\tilde{\phi}_j\rangle\right) =$$
$$= \sum_j c_j |\tilde{\phi}_j\rangle + \sum_{i,j} |\phi_i\rangle c_j \langle \tilde{p}_i|\tilde{\phi}_j\rangle - \sum_{i,j} |\tilde{\phi}_i\rangle c_j \langle \tilde{p}_i|\tilde{\phi}_j\rangle = \sum_j c_j |\phi_j\rangle = |\psi\rangle$$

since $\langle \tilde{p}_i | \tilde{\phi}_j \rangle = \delta_{i,j}$. Finally the wavefunctions $|\psi\rangle$ can be written as:

$$|\psi\rangle = \hat{T}|\tilde{\psi}\rangle = |\tilde{\psi}\rangle + \sum_i (|\phi_i\rangle - |\tilde{\phi}_i\rangle) \langle \tilde{p}_i|\tilde{\psi}\rangle \tag{4.6}$$

where it is shown that the real wavefunction is made by a first term that considers the pseudo-wavefunction all over the space, a second term which adds the real wavefunctions for the electrons close to the nuclei and a third term that removes the spherical part close to the nuclei of the pseudo-wavefunctions in order to avoid double counting. These pseudo-wavefunctions have no physical meaning inside the effective core radius.
VASP uses pseudopotentials of type PAW and the exchange and correlation potential is obtained with a particular type of GGA called *Perdew-Burke-Ernzerhof (PBE)*.

4.3 VASP input and output files

In order to perform the self consistent calculations VASP needs four input files:

- POSCAR: Defines the structure of the crystal. First are specified the basis vectors of the unit cell of the crystal in Angstrom units, then all the elements in the unit cell with their positions inside the cell. These positions can both be expressed in direct coordinates (as fractions of the basis vectors) or in Cartesian coordinates. The POSCAR file used for the calculations of CsV_3Sb_5 is shown in Fig. 4.2a;
- KPOINTS: Specifies the k-points grid used to perform calculations of quantities such as the one in eq. 3.14. The one used in this thesis was a grid 12x12x12;
- POTCAR: Includes the pseudopotentials of the atomic species specified in the POSCAR file. These pseudopotentials are known for the single atoms and need to be concatenated in the same order in which the elements are defined in the POSCAR file;
- INCAR: Includes the necessary instructions for performing the calculations. The commands used, with their explanations are shown in Fig. 4.2b.

```
New structure
1.0
       5.4944496155         0.0000000000         0.0000000000
      -2.7472248077         4.7583329468         0.0000000000
       0.0000000000         0.0000000000         9.8789911270
   Cs    V   Sb
    1    3    5
Cartesian
     0.000000000         0.000000000         0.000000000
     1.373612404         2.379166473         4.939495564
     2.747224808         0.000000000         4.939495564
    -1.373612404         2.379166473         4.939495564
     0.000000000         0.000000000         4.939495564
     2.747224893         1.586111028         7.202928248
    -0.000000003         3.172221776         2.676062879
    -0.000000003         3.172221776         7.202928248
     2.747224893         1.586111028         2.676062879
```

(a) *POSCAR file used*

```
SYSTEM = CsV3Sb5

ENCUT = 500
ISMEAR = 0
SIGMA  = 0.01
NCORE = 16
KPAR = 2
LREAL= F

LMAXMIX = 4

MAXMIX = 40 ; NELM = 200 ; EDIFF = 1.E-6

LORBIT=11
NEDOS=3000
NWRITE = 3
```

(b) *INCAR file used*

Figure 4.2: *In the INCAR file ENCUT specifies the cutoff energy from expression 4.2 in eV, ISMEAR=0 sets a Gaussian "noise" with standard deviation indicated by SIGMA which allows to make the occupation of the Kohn-Sham states continuous inside the first BZ, EDIFF specifies the highest difference in the total energies of two consecutive iterations, in eV, in order to consider convergence reached.*

The self-consistent calculations will produce different output files. The most important are: the OUTCAR file, which includes every iteration of the self-consistent cycle, including total energy, Fermi energy and energy eigenvalues, and the CHGCAR file, which stores the charge density and the PAW one-center occupancies.

For structural relaxation calculations the input files are basically the same, but some more commands needs to be included in the INCAR file:

- NSW: Specifies the highest number of ionic steps for relaxation, which was chosen to be set to 100;
- EDIFFG: specifies the convergence criteria for the relaxation procedure and can be greater than zero, for a convergence criteria on the total energy (eV) or lower than zero, for a convergence criteria on the total force (eV/Å). This was set to -10^{-3}eV/Å.
- IBRION=2: specifies the algorithm used for the relaxation procedure, in this case *conjugate gradient algorithm*;
- ISIF=3: specifies that not only the atomic positions need to be relaxed, but also the volume of the unit cell, implying that the relaxation procedure will also modify the basis vectors.

After a relaxation procedure the new coordinates are shown in a file named CONTCAR and the OUTCAR file will also include the total forces on the atoms at each iteration. In some cases the relaxation procedure is not able to reach convergence after the first calculation, so a new calculation need to be performed with the obtained CONTCAR file as the new POSCAR.

For band structures calculations one more input file is needed, which is the CHGCAR file produced with the self consistent calculation. In order to specify that the charge density must be read from this file and not calculated, the INCAR file must include the

command ICHARG=11. In addition to this also the number of energy bands that are required to be calculated can be specified with the command NBANDS, which was set to 58 for the case studied. Also the KPOINTS file needs to be modified and needs to specify the path followed in the BZ to perform the calculations and the number of points for each band (Fig. 4.3). After this the bands points to plot were obtained with the software *vaspkit.1.3.5* [17].

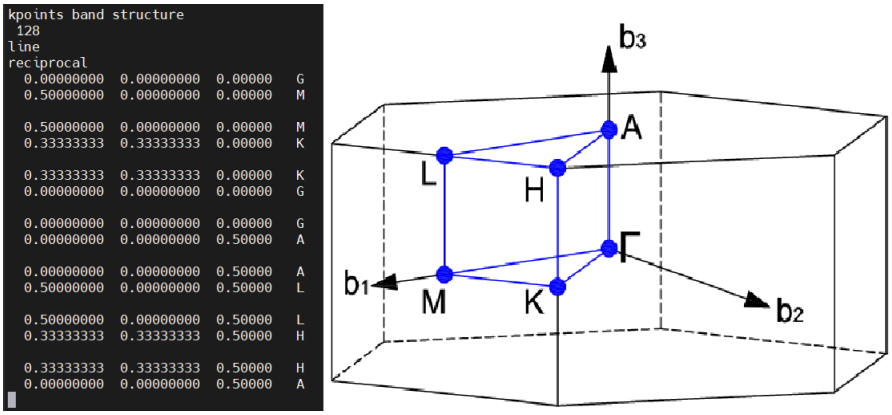

Figure 4.3: *KPOINTS file used for the calculations of energy bands (left). 128 is the number of points for band and the positions of the k-points indicated in the KPOINTS file as fractions of the basis vectors are shown inside the BZ on the right.*

4.4 Doping implementation

4.4.1 Linear interpolation of equilibrium positions

Doping a material means introducing impurities of other elements in some percentages. In particular, in the cases studied, the Sb atoms were substituted with Sn atoms, which have one less valence electron (*hole doping*) and Te atoms, which have one more valence electron (*electron doping*).
The 5 Sb atoms in CsV_3Sb_5 are symmetrically distinct, indeed one can distinguish the Sb atom within the kagome plane from the 4 above and below the kagome plane. This two different *Wyckoff positions* of the Sb atoms are not equally replaced by the doping atoms as shown in the work of *Yuzuki M. Oey et al.* [18]. In this thesis the dopants were treated as if they replaced only the 4 Sb atoms above and below the kagome plane, since these four atoms are all associated to the same *Wyckoff position*, which means that their substitution has a more significant effect with respect to what one would observe substituting only the Sb atom within the kagome plane (the doping analysis could be continued even considering uniform doping which influences also the other *Wyckoff Position*).
When changing the chemical species inside a crystal also the forces acting on each nuclear site changes, since the number of electrons is changing. In order to obtain a more accurate POSCAR, a linear interpolation of equilibrium positions was performed . This means that, starting from the relaxed unit cell of CsV_3Sb_5, where the positions of atoms can be labeled by $\vec{r}_i$, the unit cells of the crystals with a doping percentage of 100% (CsV_3SbSn_4 and CsV_3SbTe_4) were considered and structural relaxation was performed on them, obtaining new position $\vec{r}_f$ (Fig. 4.4).

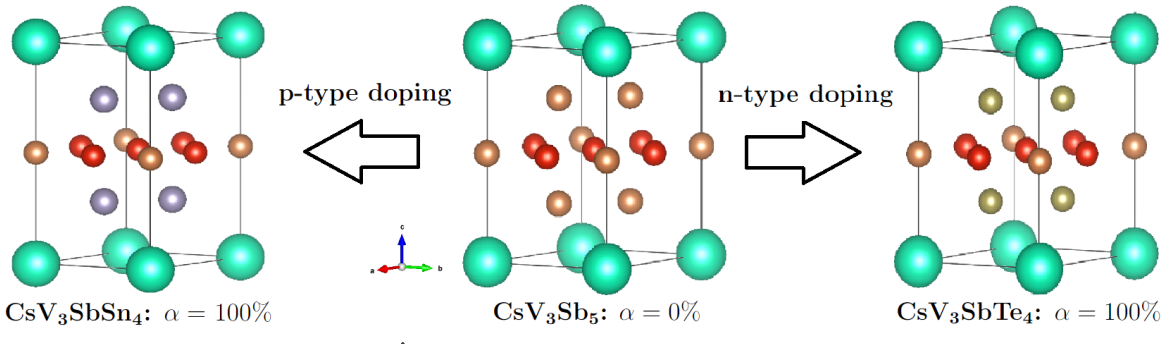

Figure 4.4: *Changes in the unit cell of CsV_3Sb_5 after hole doping with Sn atoms (represented by silver spheres) and electron doping with Te (represented by gold spheres). α is the doping percentage, and for CsV_3SbSn_4 and CsV_3SbTe_4 corresponds to 100%.*

The new equilibrium positions obtained with this procedure are shown in Fig 4.5.

```
New structure
1.0
        5.3484907150          0.0000000000          0.0000000000
       -2.6742453575          4.6319288311          0.0000000000
        0.0000000000          0.0000000000         10.4537782669
   Cs    V   Sb   Sn
    1    3    1    4
Cartesian
     0.000000000          0.000000000          0.000000000
     1.337122679          2.315964416          5.226889133
     2.674245358          0.000000000          5.226889133
    -1.337122679          2.315964416          5.226889133
     0.000000000          0.000000000          5.226889133
     2.674245440          1.543976322          7.629463283
    -0.000000003          3.087952370          2.824314984
    -0.000000003          3.087952370          7.629463283
     2.674245440          1.543976322          2.824314984
```

(a) CsV_3SbSn_4

```
New structure
1.0
        5.7698726654          0.0000000000          0.0000000000
       -2.8849363327          4.9968563048          0.0000000000
        0.0000000000          0.0000000000          9.1134653091
   Cs    V   Sb   Te
    1    3    1    4
Cartesian
     0.000000000          0.000000000          0.000000000
     1.442468166          2.498428152          4.556732655
     2.884936333          0.000000000          4.556732655
    -1.442468166          2.498428152          4.556732655
     0.000000000          0.000000000          4.556732655
     2.884936422          1.665618817          6.669396826
    -0.000000003          3.331237338          2.444068483
    -0.000000003          3.331237338          6.669396826
     2.884936422          1.665618817          2.444068483
```

(b) CsV_3SbTe_4

Figure 4.5: *Equilibrium positions of the kagome unit cell with 100% doping of Sn and Te.*

After this the positions in the unit cell with doping percentage indicated by α (in the cases studied: $\alpha = 1\%, 2\%, 5\%, 10\%$ for both Sn and Te) can be approximated by the linear relation:

$$\vec{r}_\alpha = (\vec{r}_f - \vec{r}_i)\alpha + \vec{r}_i$$

where the positions must be in Cartesian coordinates.
In this procedure also the volume of the unit cell was allowed to be modified (command ISIF=3 in the INCAR file).

4.4.2 Virtual Crystal Approximation

The two most used methods in order to reproduce impurities in materials are the *supercell method* and the *Virtual Crystal Approximation (VCA)*.
The supercell method consists in reproducing the impurity studying not the single unit cell of the material, but a bigger cell composed by more unit cells. Substitutions are then performed in just some single cells of this agglomeration of cells, in order to mimic the distributions of the impurities. The supercell is then repeated periodically in space, so that the impurities become a periodical property of the crystal. However this method can be computationally demanding and, in addition to this, increasing the size of the

unit cell considered in the calculations reduces the size of the BZ, which means that the bands obtained will be folded.

VCA was chosen as the method to introduce doping in this thesis because of its effectiveness [19][20] and its reasonable computational demand. This method consists in studying a crystal with the same periodicity of the one without impurities, but composed of fictitious "virtual" atoms that interpolate between the behaviour of the original atoms and the impurity atoms.
The application of VCA is related to the use of pseudopotentials. Indeed, for local pseudopotentials, considering a crystal made of two elements A and B, with an atom C substituted to atom B with an impurity percentage x, the VCA pseudopotential is obtained averaging the potentials of the AB and AC compounds:

$$V_{VCA}(\vec{r}) = (1-x)V_{AB}(\vec{r}) + xV_{AC}(\vec{r})$$

In practice this is usually done in Fourier space by averaging $V_{AB}(\vec{G})$ and $V_{AC}(\vec{G})$. The total energy of the system is given by eq. 3.5, where V_{ext} is given, in terms of the pseudopotentials V_{ps}^I, as:

$$V_{ext}(\vec{r}) = \sum_I V_{ps}^I(\vec{r} - \vec{R}_I)$$

For the pseudopotential of the element substituted by the impurity the VCA pseudopotential is obtained as:

$$V_{ps}^I(\vec{r}) = (1-x)V_{ps}^B(\vec{r}) + xV_{ps}^C(\vec{r})$$

while, for the element unaffected by the impurities the pseudopotential remains:

$$V_{ps}^I(\vec{r}) = V_{ps}^A(\vec{r})$$

With these considerations V_{ext} for VCA becomes:

$$V_{ext}(\vec{r}) = \sum_I \sum_\alpha w_\alpha^I V_{ps}^\alpha(\vec{r} - \vec{R}_{i,\alpha})$$

where w_α^I are the weights which specifies the statistical composition of site I and, in the previous example, would be 1 for specie A, $(1-x)$ for specie B and x for specie C. One can thus think of the new crystal as composed by the normal atoms that are not substituted by the impurities and some "ghost" atoms which are the impurities elements and the original ones, which share the same lattice positions, with weights x and $(1-x)$. For CsV_3Sb_5 the doped unit cell exposed in the previous section would thus include 1 Cs atom, 3 V atoms, 5 Sb atoms (1 "standard" and 4 "ghosts") and 4 doping "ghost" atoms (Sn or Te), which would share the same positions of the 4 Sb atoms above and below the kagome plane with weights x and $(1-x)$ where x is the doping percentage. The changes in the POSCAR file in order to introduce this behaviour are shown in Fig. 4.6 for 1% doping of Sn, while in order to practically introduce this behaviour with a POTCAR file one needs to include the pseudopotentials of each "standard" atom and of each "ghost" atom (this means that, for the case studied, the pseudopotential of Sb needed to be included twice, once for the Sb atoms in the kagome plane and a second time for the other four Sb atoms).

With this method also the valence of the sites with impurities changes and becomes, for site I:

$$\bar{Z}_I = \sum_\alpha w_\alpha^I Z_\alpha$$

So the implementation of VCA requires to substitute this valence and remove the infinities on site interaction terms due to the Coulomb repulsion between two "ghost" atoms which share the same site.

```
New structure
1.0
        5.492990026     0.000000000     0.000000000
       -2.746495013     4.757068906     0.000000000
        0.000000000     0.000000000     9.884738998
   Cs    V   Sb   Sb   Sn
    1    3    1    4    4
Cartesian
     0.000000000     0.000000000     0.000000000
     1.373247507     2.378534452     4.942369500
     2.746495014     0.000000000     4.942369500
    -1.373247507     2.378534452     4.942369500
     0.000000000     0.000000000     4.942369500
     2.746495098     1.585689681     7.207193598
    -0.000000003     3.171379082     2.677545400
    -0.000000003     3.171379082     7.207193598
     2.746495098     1.585689681     2.677545400
     2.746495098     1.585689681     7.207193598
    -0.000000003     3.171379082     2.677545400
    -0.000000003     3.171379082     7.207193598
     2.746495098     1.585689681     2.677545400
```

Figure 4.6: *Changes introduced in the POSCAR file for the 1% doping percentage of Sn in order to use VCA, with positions obtained with the procedure explained in section 4.4.1.*

This method allowed to study different doping levels without further changes to the POSCAR and the POTCAR files, but only specifying the different doping percentages w_I in the INCAR file with the command VCA (Fig. 4.7).

```
VCA = 1 1 1 0.99 0.01
```

Figure 4.7: *Command used in the INCAR file in order to introduce the 1% level of doping. The five numbers represent the weights of the different atomic species and are, in order Cs, V and the Sb atom in the kagome plane, which are unchanged by VCA, Sb and the Sn (or Te) atoms, which are the "ghost" atoms with weights different from 1.*

It is important to notice that the order in which the elements are considered in the POSCAR, POTCAR and INCAR (for the VCA command) files is important and needs to be same in all of them, as it can be seen comparing Fig. 4.6 and Fig. 4.7.

Chapter 5

Results

5.1 Results for CsV_3Sb_5

5.1.1 Energy bands

Fig. 5.1 shows the bands obtained with VASP for CsV_3Sb_5. These bands results compatible with those reported in Fig. 1.11 obtained by [10]. The important features that can be observed are the VHs at the M point and the Dirac crossings at the K and H points, as well as the Dirac cones between the K and Γ points and between the H and A points and the electron pocket at the Γ point. The DFT calculations performed were thus able to reproduce the properties obtained by other studies [9] [10], summarized in Chapter 1.

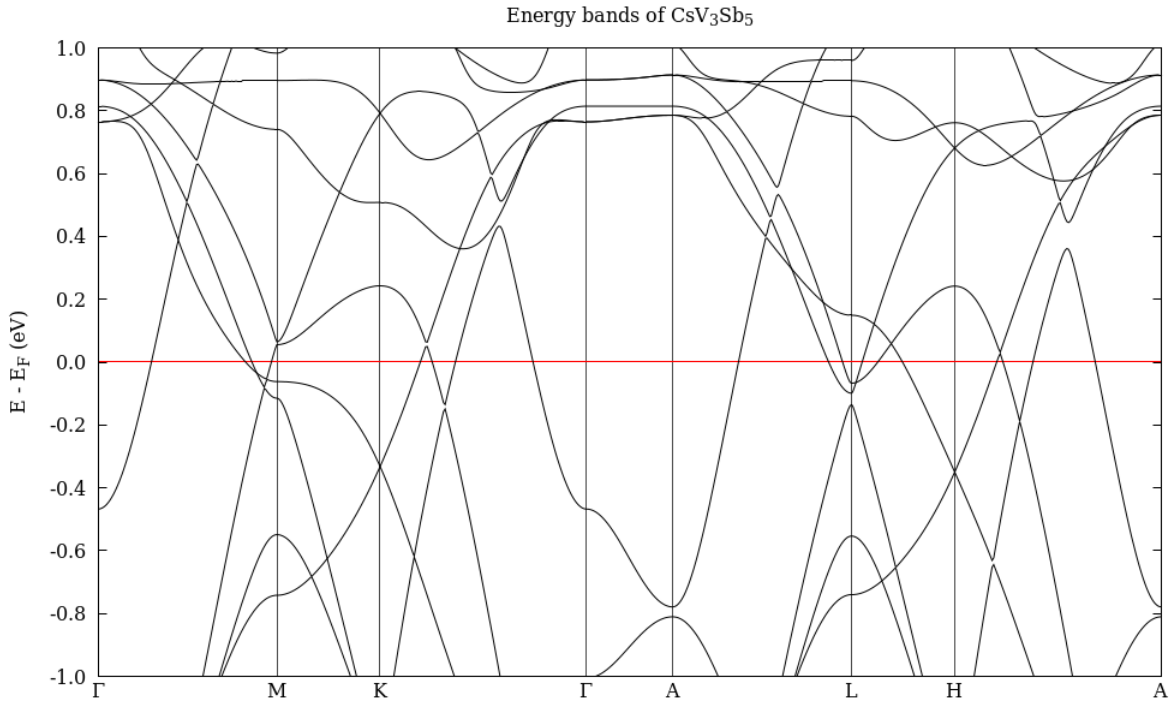

Figure 5.1: *DFT result for the energy bands of CsV_3Sb_5 obtained with VASP. The red horizontal line marks the Fermi level, which was shifted in order to coincide with the 0.0eV of the vertical axis. On the horizontal axis the high symmetry points of the BZ are marked and are the same shown in Fig. 4.3.*

Further analysis can be done considering the contributions of the three elements of the crystal (Cs, V and Sb) to the energy bands, shown in Fig. 5.2. The behaviour is the expected one and is compatible with what was shown in Fig. 1.7.

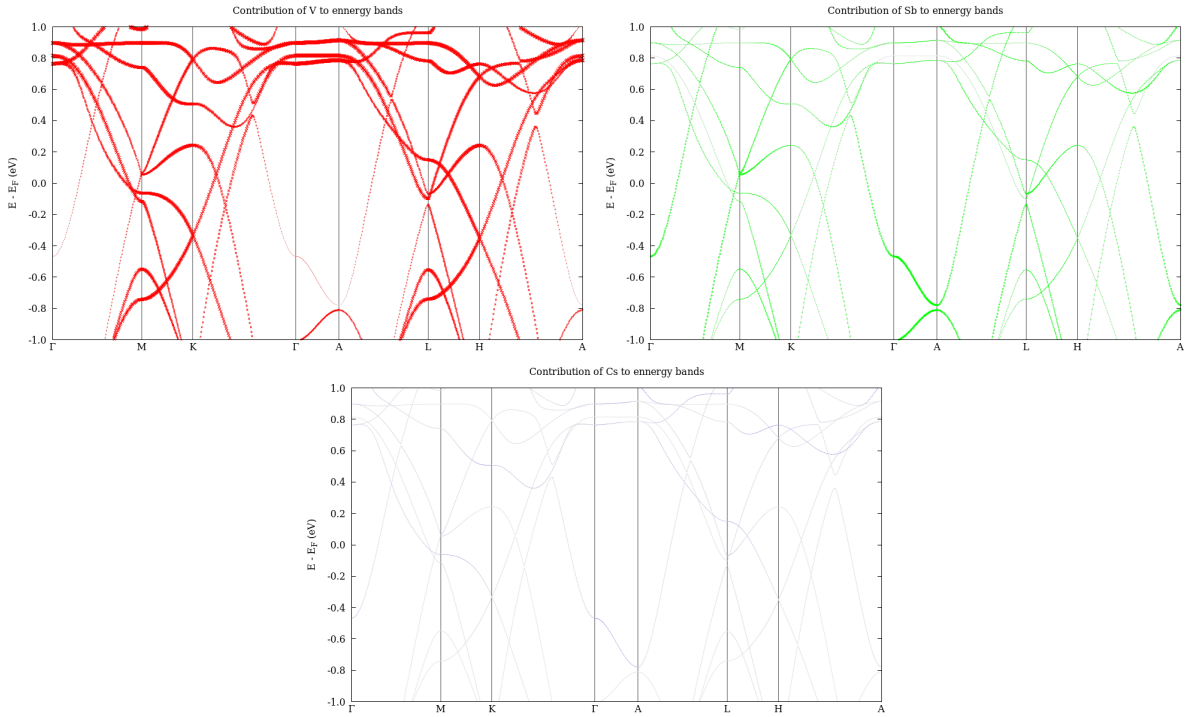

Figure 5.2: *Contribution of the different elements of CsV_3Sb_5 to the energy bands. Red dots mark the contribution of V, green dots of Sb and blue dots of Cs while grey lines are the energy bands of CsV_3Sb_5 shown in Fig. 5.1. The larger are the dots of a specific element at a certain point the greater is its contribution to that specific part of that band.*

The electron pocket at the Γ point is generated by the Sb $p-orbitals$, the VHs that appears slightly above the Fermi level is derived from a mixture of the V $d-orbitals$ and Sb $p-orbitals$, while the one below the Fermi level is mainly due to the contribution of V $d-orbitals$, all features reported also by [9] and [10]. The role of Cs, instead, is, as one would expect, negligible with respect to the other elements, since its role is mainly structural, and contributes significantly only to high-energy bands, which do not play a role in the properties that are considered of interest of CsV_3Sb_5.

5.1.2 Density of States

Considering now the graph obtained for the Density of States, shown in Fig. 5.3, one can notice that this has two peaks in proximity of the Fermi level, which correspond to the expected logarithmic divergence of the Density of States at the two VHs above and below the Fermi level[1] which can be observed in Fig. 5.1.

[1]The VHs in the density of states behave as peaks and not logarithmic singularities since this behaviour is expected for exactly bi-dimensional materials, while the crystal studied is actually 3-dimensional, so that it does not have the logarithmic divergence of the density of states at the saddle points [2] and behaves as bi-dimensional only as a first approximation.

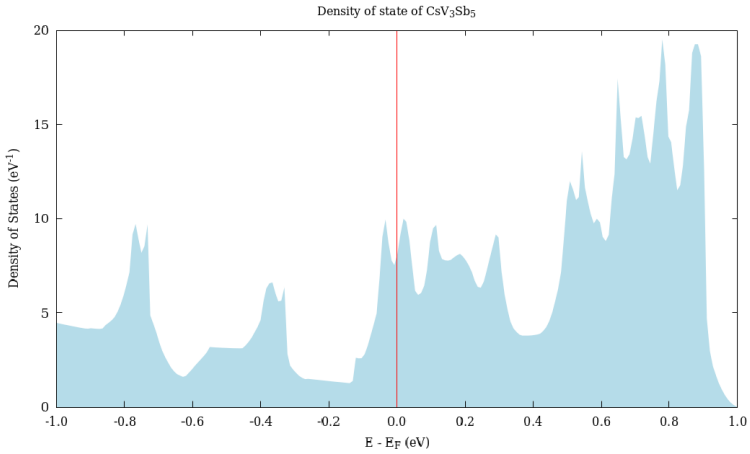

Figure 5.3: *DFT result for the density of states of CsV_3Sb_5 obtained with VASP. The red vertical line marks the Fermi level, which was shifted in order to coincide with the 0.0eV of the horizontal axis.*

5.2 Doping results

Fig. 5.4 shows the behaviour of the energy bands under the effect of Sn (green bands) and Te (blue bands) doping, implemented as explained in section 4.4. As one would expect the effect of *hole-doping* (Sn) moves the energy bands upwards with respect to the original bands of CsV_3Sb_5, while *electron-doping* (Te) has the opposite effect.

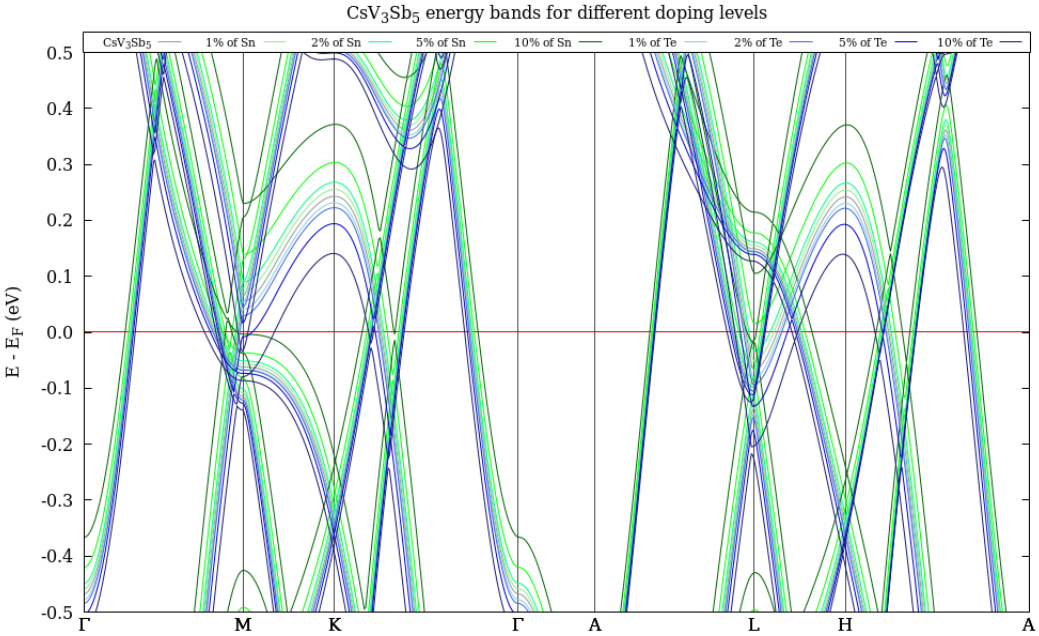

Figure 5.4: *DFT result for the energy bands of CsV_3Sb_5 with different doping levels obtained with VASP. The red horizontal line marks the Fermi level, which was shifted in order to coincide with the 0.0eV of the vertical axis. Different colors mark the different types of doping, with Sn doping shown by green bands and Te doping by blue bands, while the bands for CsV_3Sb_5 without doping are shown in grey for comparison. For both the types of doping the bands colors get darker increasing the doping percentage.*

Considering the VHs of *m-type* at the M point slightly above the Fermi level, one can notice that Te doping moves the VHs towards E_F, which is reached for a doping percentage of 5% and crossed for a doping percentage of 10%. A similar behaviour is shown by the VHs at the L point, which, under Sn doping, gets closer to E_F, crossing it for doping percentages greater than 5%. The effect of Sn doping on CsV_3Sb_5 has already been studied by *Yuzuki M. Oey et al.* [18] and has been observed to lead to a suppression of Charge Density Wave state and a modulation of the critical temperature with a double dome behaviour.

Fig. 5.5 shows highlights on the two doping percentages previously mentioned, in order to visualize better the displacement of the two VHs considered.

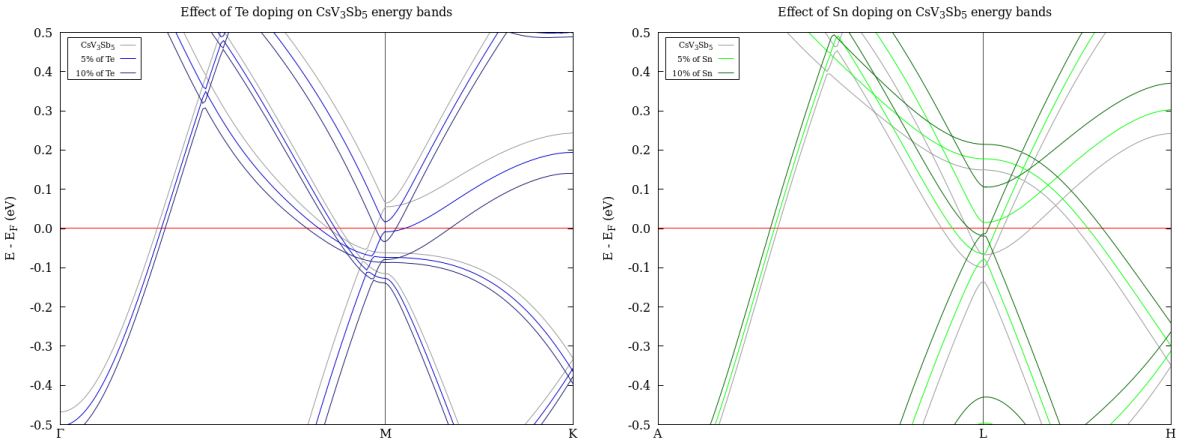

Figure 5.5: *Highlights of the effects of the highest doping percentages of Te and Sn. The red horizontal line marks the Fermi level, which was shifted in order to coincide with the 0.0eV of the vertical axis. Te doping is shown in blue on the left, while Sn doping is shown in green on the right.*

Since in the procedure shown in section 4.4.1 for relaxation also the volume of the unit cell was allowed to change also the reciprocal lattice vectors will have changed for the different levels of doping, since they depend on the real lattice vectors. This shift of the k-points with respect to those of CsV_3Sb_5 was quantified for the different levels of doping, with a highest observed displacement of $\sim 0.015 Å^{-1}$ for the A point of the 10% doping of Te, while, for the M and L points of the two VHs previously considered this shift was of $\sim 0.0033 Å^{-1}$ and $\sim 0.0098 Å^{-1}$ respectively (always referred to the 10% doping of Te, which was associated to the greatest shifts for all the k-points). These amounts are negligible to be represented in the graphs, since they do not affect much the positions of the VHs considered on the horizontal axis. Because of this the k-points labeled in the graphs are always referred to the k-points of CsV_3Sb_5 without doping.

In order to verify that these effects are actually related to doping and not to the structural modulation explained in section 4.4.1 (since changes in the unit cell and in the positions of the atoms also have a role in the modulation of the energy bands) a comparison graph with the bands of CsV_3Sb_5 without doping, but with the atomic positions and the unit cells of the different doping levels was realised. This allowed to consider the displacement of the energy bands due only to the structural modulation and not to the doping and is shown in Fig. 5.6.

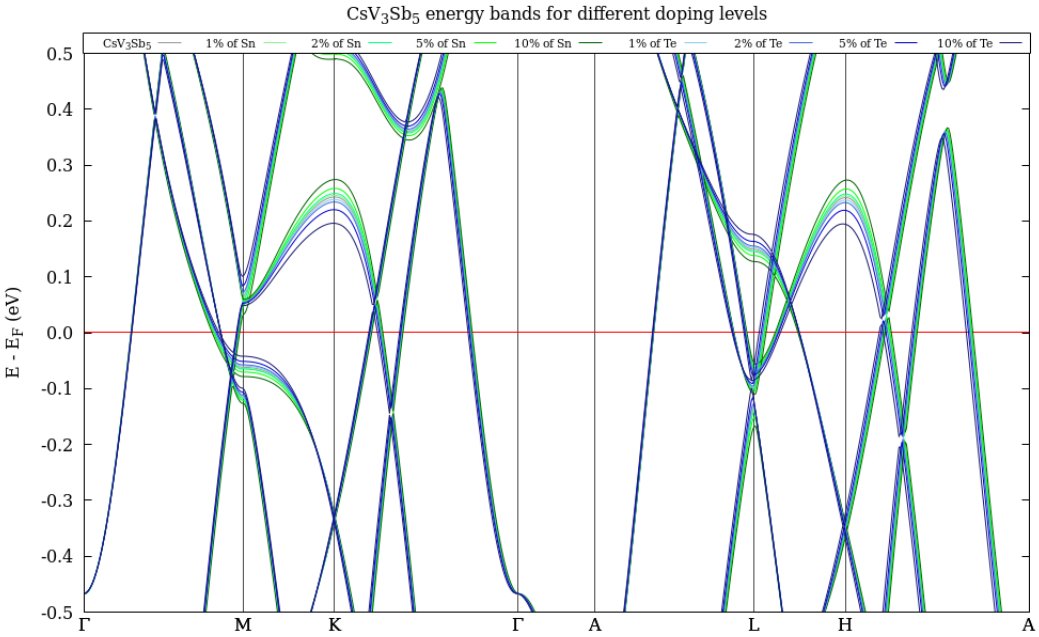

Figure 5.6: *DFT result for the energy bands of CsV_3Sb_5 without doping but with the different dimensions of the unit cell and the different positions of the atoms obtained in section 4.4.1 for the different doping levels obtained with VASP. The red horizontal line marks the Fermi level, which was shifted in order to coincide with the 0.0eV of the vertical axis. Different colors mark which doping percentage is represented by the different positions used and the colors used are the same used in Fig. 5.4, with Sn doping positions shown by green bands and Te doping positions by blue bands, while the bands for CsV_3Sb_5 with the original positions are shown in grey for comparison.*

Fig. 5.6 shows that the displacement due only to the structural modulation is much less intense than the one observed before and is not enough for the bands to reach E_F for both the VHs previously considered, proving that the effect is mainly due to doping.

Moving the VHs toward the Fermi level might have an effect on the interplay between the Charge Density Wave state and the superconducting state in CsV_3Sb_5, but, since DFT only allows to study the modulation of the energy bands, but not the effect that these modulations have on the many-body properties of materials, further studies need to be carried out, with different theoretical or experimental methods.

Conclusions

The work carried out in this thesis effectively succeeded in reproducing results obtained by other studies which have already encountered experimental evidence [9] [10] for kagome metal CsV_3Sb_5. In particular the obtained band structure correctly shows the expected VHs and other properties such as the Dirac cones and crossings. Also analyzing the different contributions of the different elements of the material and their orbitals yielded results already obtained in the previously mentioned studies. These results show that VASP and *Density Functional Theory* are effective tools for studying this kind of materials with first principle calculations, allowing to make predictions for some of their properties.
As far as doping is concerned, the results obtained show that electron doping, for doping percentages above 5%, succeeds in shifting below the Fermi level the VHs at the M point of the band structure slightly above the Fermi level, while hole doping, always for doping percentages greater that 5%, succeeds in shifting above the Fermi level the VHs at the L point. These effects were also proved to be mainly due to the actual change in the number of the electrons related to doping rather than to the modulation of the atomic positions due to the substitution of the atomic species, whose effect was proved to be negligible for the interesting points. These results take part in an open field of study and might have a role in the interplay between charge density wave and superconductivity in this material. The effect that these shifts of the energy bands will have on the many-body properties of the material requires more specific studies, with theoretical tools that can use beyond DFT methods or experimental approaches. In addition to this, experimental evidence or confutation of these results could also help understanding the effectiveness of VCA for this kind of studies and if it is actually a reliable tool for the implementation of doping effects.

Bibliography

[1] Kittel, C. (2004). Introduction to solid state physics (8th ed.). John Wiley & Sons.

[2] Bassani, F.; Pastori Parravicini, G. (1975). Electronic States and Optical Transitions in Solids. Pergamon Press. ISBN 978-0-08-016846-3.

[3] Van Hove, Léon (15 March 1953). "The Occurrence of Singularities in the Elastic Frequency Distribution of a Crystal". Physical Review. 89 (6). American Physical Society (APS): 1189–1193.

[4] Zhao, Guang-Lin & Bagayoko, Diola. (2007). A universal relation between the densities of states near van Hove singularities and the effective electron masses in 1-dimensional materials. International Journal of Modern Physics B. 21. 10.1142/S0217979207044779.

[5] G. D. Mahan, Many-particle physics. Springer Science & Business Media, 2000.

[6] Carsten T. (2023). Theory of Superconductivity. URL: `https://tu-dresden.de/mn/physik/itp/cmt/ressourcen/dateien/skripte/Skript_Supra.pdf?lang=en`

[7] Furuya, Shunsuke & Horinouchi, Yusuke & Momoi, Tsutomu. (2020). Anomalies of kagome antiferromagnets on magnetization plateaus.

[8] Norman, M. R. (2016). Herbertsmithite and the Search for the Quantum Spin Liquid. arXiv.Org. `https://doi.org/10.48550/arxiv.1604.03048`.

[9] Wilson, S. D., & Ortiz, B. R. (2023). AV_3Sb_5 Kagome Superconductors: Progress and Future Directions. `https://doi.org/10.48550/arxiv.2311.05946`.

[10] Kang, M., Fang, S., Kim, J.-K., Ortiz, B. R., Ryu, S. H., Kim, J., Yoo, J., Sangiovanni, G., Di Sante, D., Park, B.-G., Jozwiak, C., Bostwick, A., Rotenberg, E., Kaxiras, E., Wilson, S. D., Park, J.-H., & Comin, R. (2022). Twofold van Hove singularity and origin of charge order in topological kagome superconductor CsV_3Sb_5. Nature Physics, 18(3), 301–308.

[11] Consiglio, A., Schwemmer, T., Wu, X., Hanke, W., Neupert, T., Thomale, R., Sangiovanni, G., & Domenico Di Sante. (2021). Van Hove tuning of AV3Sb5 kagome metals under pressure and strain. arXiv.Org. `https://doi.org/10.48550/arxiv.2111.09342`.

[12] Wu, X., Schwemmer, T., Müller, T., Consiglio, A., Sangiovanni, G., Di Sante, D., Iqbal, Y., Hanke, W., Schnyder, A. P., Denner, M. M., Fischer, M. H., Neupert, T., & Thomale, R. (2021). Nature of unconventional pairing in the kagome superconductors AV_3Sb_5. `https://doi.org/10.48550/arxiv.2104.05671`.

[13] Yu, F. H., Ma, D. H., Zhuo, W. Z., Liu, S. Q., Wen, X. K., Lei, B., Ying, J. J., & Chen, X. H. (2021). Unusual competition of superconductivity and charge-density-wave state in a compressed topological kagome metal. Nature Communications, 12(1), 3645–3645. https://doi.org/10.1038/s41467-021-23928-w.

[14] F. Giustino. Materials Modelling Using Density Functional Theory: Properties and Predictions. Oxford University Press, 2014. ISBN: 9780199662449.

[15] Blundell, S. J. (2023). Density functional theory: a practical introduction, 2nd edition, by David S. Sholl and Janice A. Steckel, Hoboken, NJ, Wiley, 2023, 204 pp., ISBN 978-1119840862.

[16] VASP wiki: https://www.vasp.at/wiki/index.php/The_VASP_Manual.

[17] vaspkit software: https://vaspkit.com/.

[18] Oey, Y. M., Ortiz, B. R., Kaboudvand, F., Frassineti, J., Garcia, E., Cong, R., Sanna, S., Mitrović, V. F., Seshadri, R., & Wilson, S. D. (2022). Fermi level tuning and double-dome superconductivity in the kagome metal $CsV_3Sb_{5-x}Sn_x$, Physical Review Materials, 6(4).

[19] Bellaiche, L., & Vanderbilt, D. (1999). The virtual crystal approximation revisited: Application to dielectric and piezoelectric properties of perovskites. https://doi.org/10.48550/arxiv.cond-mat/9908364.

[20] Ramer, N. J., & Rappe, A. M. (1999). Virtual-crystal approximation that works: Locating a composition phase boundary in $Pb(Zr_{1-x}Ti_3)O_3$. https://doi.org/10.48550/arxiv.cond-mat/9909032